



## Article

# Novel and Potent Acetylcholinesterase Inhibitors for the Treatment of Alzheimer's Disease from Natural ( $\pm$ )-7,8-Dihydroxy-3-methyl-isochroman-4-one

Xinnan Li <sup>1</sup>, Yilin Jia <sup>1</sup>, Junda Li <sup>1</sup>, Pengfei Zhang <sup>1</sup>, Tiantian Li <sup>2</sup>, Li Lu <sup>2</sup> , Hequan Yao <sup>1,\*</sup>, Jie Liu <sup>3,\*</sup>, Zheyong Zhu <sup>2</sup>  and Jinyi Xu <sup>1,\*</sup>

<sup>1</sup> State Key Laboratory of Natural Medicines, Department of Medicinal Chemistry, China Pharmaceutical University, Nanjing 211198, China; xinnanli@126.com (X.L.); ammie10@163.com (Y.J.); zgykdxljd0938@163.com (J.L.); zpf834220218@163.com (P.Z.)

<sup>2</sup> Division of Molecular Therapeutics & Formulation, School of Pharmacy, The University of Nottingham, University Park Campus, Nottingham NG7 2RD, UK; paytl4@nottingham.ac.uk (T.L.); Li.Lu@nottingham.ac.uk (L.L.); Zheyong.Zhu@nottingham.ac.uk (Z.Z.)

<sup>3</sup> Department of Organic Chemistry, China Pharmaceutical University, Nanjing 211198, China

\* Correspondence: hyao@cpu.edu.cn (H.Y.); cpu-jill@163.com (J.L.); jinyixu@china.com (J.X.)

**Abstract:** Alzheimer's disease (AD) is a neurodegenerative disease that causes memory and cognitive decline as well as behavioral problems. It is a progressive and well recognized complex disease; therefore, it is very urgent to develop novel and effective anti-AD drugs. In this study, a series of novel isochroman-4-one derivatives from natural ( $\pm$ )-7,8-dihydroxy-3-methyl-isochroman-4-one [( $\pm$ )-XJP] were designed and synthesized, and their anti-AD potential was evaluated. Among them, compound **10a** [(Z)-3-acetyl-1-benzyl-4-((6,7-dimethoxy-4-oxoisochroman-3-ylidene)methyl)pyridin-1-ium bromide] possessed potent anti-acetylcholinesterase (AChE) activity as well as modest antioxidant activity. Further molecular modeling and kinetic investigations revealed that compound **10a** was a dual-binding inhibitor that binds to both catalytic anionic site (CAS) and peripheral anionic site (PAS) of the enzyme AChE. In addition, compound **10a** exhibited low cytotoxicity and moderate anti-A $\beta$  aggregation efficacy. Moreover, the in silico screening suggested that these compounds could pass across the blood–brain barrier with high penetration. These findings show that compound **10a** was a promising lead from a natural product with potent AChE inhibitory activity and deserves to be further developed for the prevention and treatment of AD.

**Keywords:** Alzheimer's disease; ( $\pm$ )-7,8-dihydroxy-3-methyl-isochroman-4-one; acetylcholinesterase inhibitors; antioxidant activity; molecular docking



**Citation:** Li, X.; Jia, Y.; Li, J.; Zhang, P.; Li, T.; Lu, L.; Yao, H.; Liu, J.; Zhu, Z.; Xu, J. Novel and Potent Acetylcholinesterase Inhibitors for the Treatment of Alzheimer's Disease from Natural ( $\pm$ )-7,8-Dihydroxy-3-methyl-isochroman-4-one. *Molecules* **2022**, *27*, 3090. <https://doi.org/10.3390/molecules27103090>

Academic Editor: Jorge A. R. Salvador

Received: 12 April 2022

Accepted: 9 May 2022

Published: 11 May 2022

**Publisher's Note:** MDPI stays neutral with regard to jurisdictional claims in published maps and institutional affiliations.



**Copyright:** © 2022 by the authors. Licensee MDPI, Basel, Switzerland. This article is an open access article distributed under the terms and conditions of the Creative Commons Attribution (CC BY) license (<https://creativecommons.org/licenses/by/4.0/>).

## 1. Introduction

Alzheimer's disease (AD) is a neurodegenerative disease and the most common type of dementia with the symptoms of progressive memory loss, cognitive impairment, changes of personality, and linguistic disorders [1–3]. There are currently more than 50 million AD patients worldwide, with an estimated increase to 139 million patients by 2050, leading to a significant financial burden on families and society [4–9].

The senile plaque (SP) generated by  $\beta$ -amyloid (A $\beta$ ) and neurofibrillary tangles (NFTs) made of phosphorylated tau proteins in the hippocampus are considered as the main pathogenic etiologies of AD [10]. The pathological mechanism of AD is complex, and several hypotheses have been proposed, including cholinergic injury hypothesis [11,12],  $\beta$ -amyloid protein cascade hypothesis [13], tau protein hyperphosphorylation hypothesis [14], metal ion poisoning hypothesis [15], calcium imbalance hypothesis [16], chronic inflammation hypothesis [17], and oxygen free radical damage hypothesis [18]. Among these hypotheses, the cholinergic injury is the most widely accepted and its clinical effectiveness has been approved. In the human brain, acetylcholine functions as a cholinergic

neurotransmitter and plays an important role in cognition, learning, and memory. Over the past decades, many studies have found that a huge number of cholinergic neurons in the brains of AD patients are damaged, and the level of acetylcholine during nerve impulse transmission is greatly reduced, affecting signal transmission and leading to learning and cognitive failure [19–22]. Compelling evidence supports the concept that the shortage of acetylcholine is one of the main causes of AD, indicating that elevating acetylcholine level would improve AD patients [23].

AChE inhibitors, such as donepezil, rivastigmine, and galantamine, are the most commonly used anti-AD drugs clinically (Figure 1A) [1]. The AChE inhibitors work by binding the catalytic active site (CAS) at the bottom of AChE, leading to the increased level of acetylcholine (ACh). Recent research has found that the peripheral active site (PAS), which is located at the entrance of the AChE canyon active site, is linked to the neurotoxic cascade of AD caused by acetylcholine hydrolysis and AChE-induced  $A\beta$  aggregation [24]. Thus, dual interaction of binding sites both on CAS and PAS would lead to a better inhibitory activity against AChE for the treatment of AD [25–27]. ( $\pm$ )-7,8-Dihydroxy-3-methyl-isochroman-4-one [( $\pm$ )-XJP] (Figure 1B) is a novel and structurally distinct natural polyphenolic molecule that our group isolated from the peel of a banana (*Musa sapientum* L.) and which displays potent antihypertensive and antioxidant activities (Figure 1B) [28,29].

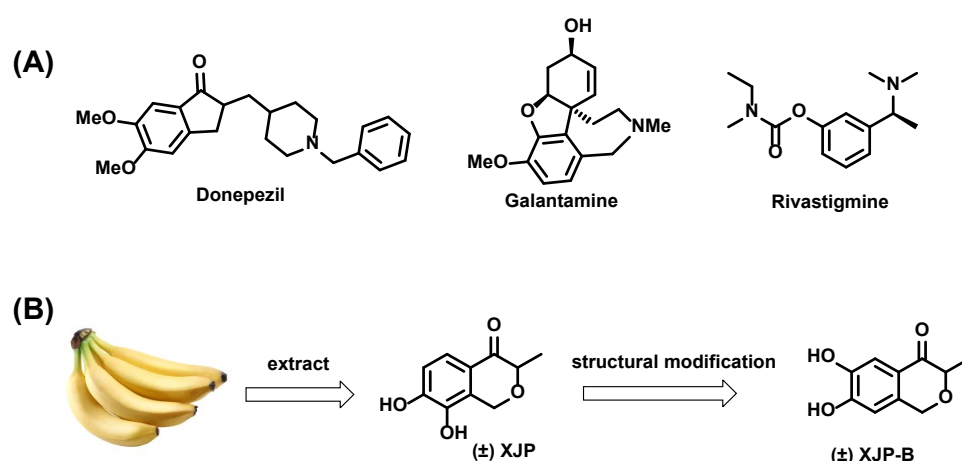


**Figure 1.** (A) The structures of AChE inhibitors donepezil, galantamine and rivastigmine; (B) The structure of ( $\pm$ )-XJP and ( $\pm$ )-XJP-B.

The indenone fragment of donepezil occupies PAS of AChE. Due to the structural similarity between indenone and isochromanone, the indenone fragment of donepezil was cleverly designed by replacing it with the isochromanone structure of ( $\pm$ )-XJP. We hoped that the isochromanone structure could occupy PAS as well. The benzyl piperidine fragment of donepezil is the key pharmacophore that occupies CAS, and, combined with our previous studies [30–32], we retained the cyclic structure of this fragment and replaced the piperidine ring with a pyridine ring. The central region of the AChE active pocket becomes narrower and consequently restricts the passage of ring structures containing larger substituents; the bottom region of the pocket becomes relatively larger and therefore contains several lateral cavities that could be further occupied to improve the affinity of a compound on AChE (Figure 2B). In a previous work [31], we fused ( $\pm$ )-XJP with a donepezil analog possessing a pyridine ring to obtain a series of new compounds with no substituents on the pyridine ring, and the most potent compound had good AChE inhibitory activity with  $IC_{50}$  value of  $21.1 \pm 0.8$  nM. On this basis, when designing new molecules, we introduced acetyl or aminocarbonyl groups that would occupy less space on the pyridine ring for the following reasons: the smaller acyl structure does not affect benzyl pyridine fragment to access CAS; and the spatial configuration of acyl group and hydrogen binding donors or acceptors that they contain has the potential to form more

interactions with the active pocket. In our previous study, the structural modification of ( $\pm$ )-XJP provided an analog of it, named ( $\pm$ )-XJP-B, which displayed more potent activity than natural ( $\pm$ )-XJP. Therefore, by fusing the pharmacophores of ( $\pm$ )-XJP-B and donepezil, we designed and synthesized thirty-five new 4-isochromanone derivatives and evaluated their AChE inhibition to investigate the potential for AD treatment (Figure 2A).

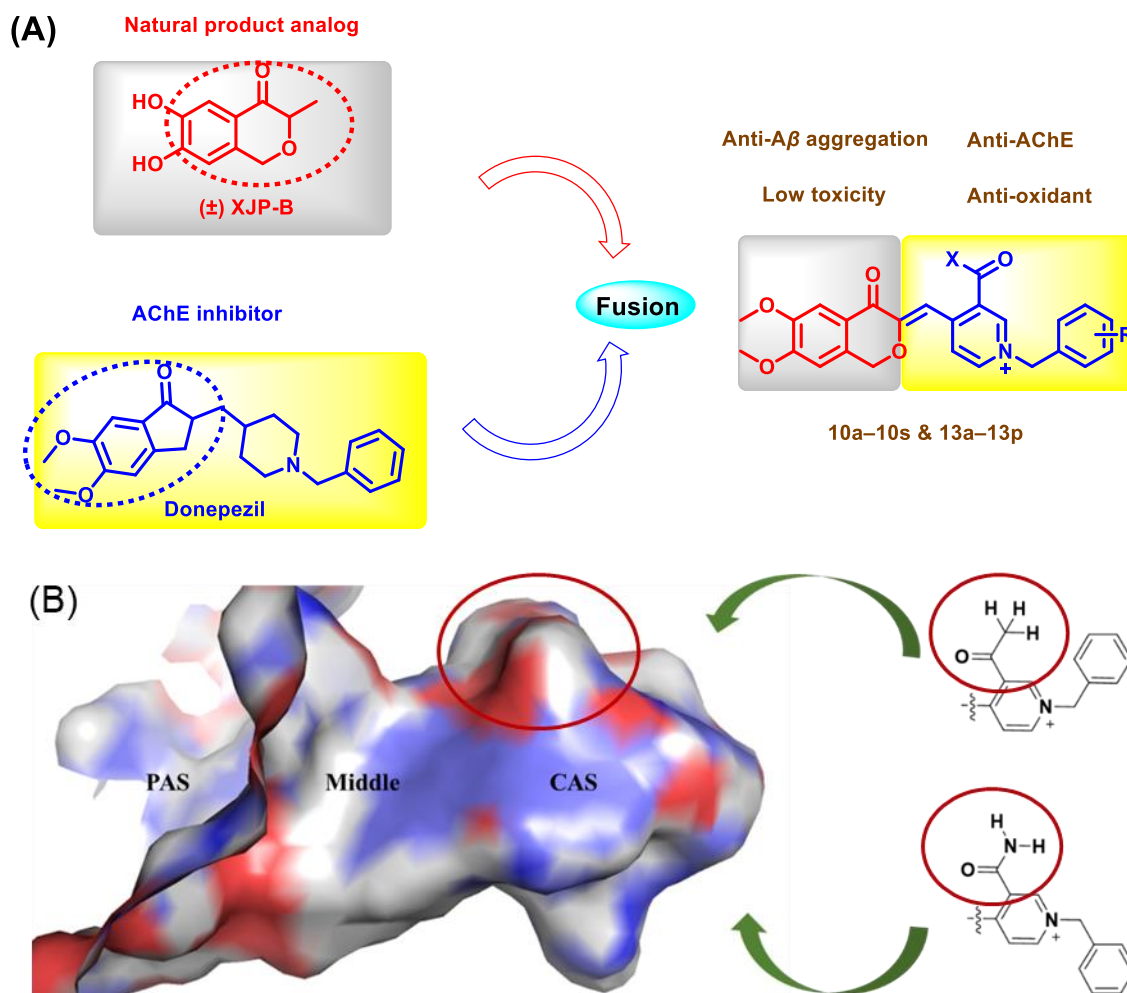


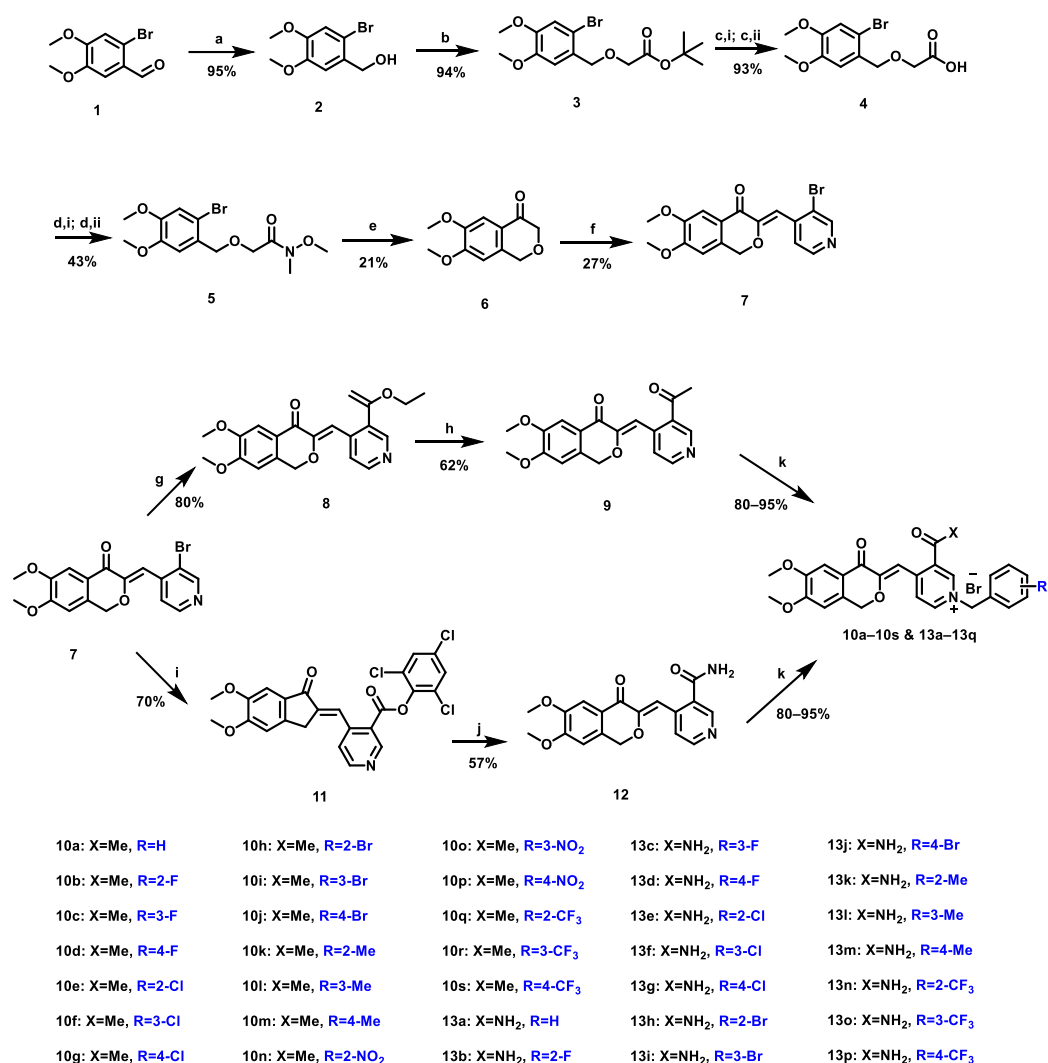
**Figure 2.** (A) Design strategy of the target compounds. (B) The pharmacophore of target compounds and the active pockets of AChE.

## 2. Results and Discussions

### 2.1. Synthesis

The synthesis of new isochroman-4-one derivatives **10a–10s** and **13a–13p** is depicted in Scheme 1. Briefly, the synthetic route is divided into two parts: the first part is synthesis of key intermediate **7**, and the second part is synthesis of the target compounds. Firstly, commercially available **1** was reduced under the action of sodium borohydride to obtain intermediate **2**, then intermediate **2** was etherified with tert-butyl bromoacetate under two-phase environment and alkaline conditions to obtain intermediate **3**. In the presence of a strong base, alcoholysis of ester and hydrolysis of ester occurred successively to produce intermediate **4**. Under the action of oxalyl chloride, **4** produced the corresponding acid chloride, which was reacted with *N,O*-dimethylhydroxylamine hydrochloride to yield Weinreb amide intermediate **5**. In an anhydrous, oxygen-free and low temperature environment, **5** underwent intramolecular condensation under the action of tert-butyl lithium to obtain XJP derivative **6**; intermediate **6** was condensed with bromopyridinecarboxaldehyde under high temperature conditions to obtain key intermediate **7**. The bromine substituent on the

pyridine ring of intermediate 7 could be reacted with tributyl(1-ethoxyethylene) tin under the catalysis of bis-dibenzylideneacetone palladium to obtain intermediate 8, placed in a strong acid environment, which can be converted to intermediate 9 through enols; finally, with different substituted benzyl bromide under high temperature conditions to generate target compounds 10a–10s. Under the catalysis of palladium acetate and xantphos phosphorus ligand, the bromine group on intermediate 7 was replaced by 2,4,6-trichlorophenyl formate to form ester intermediate 11. In a closed environment of high temperature and pressure, 11 led to the aminolysis reaction of ester yielding intermediate 12. Similarly, it reacted with different substituted benzyl bromides in dried acetonitrile under reflux to yield the target compounds 13a–13p. All target compounds were characterized by  $^1\text{H}$  NMR,  $^{13}\text{C}$  NMR, and HR-ESI-MS.

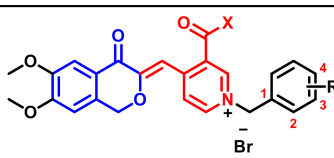


**Scheme 1.** Reagents and conditions: (a)  $\text{NaBH}_4$ , MeOH,  $0^\circ\text{C}$ , 20 min; (b) tert-butyl bromoacetate, tetrabutylammonium bromide, KOH in  $\text{H}_2\text{O}$ , toluene,  $50^\circ\text{C}$ , 1 h; (c,i) MeONa, MeOH, r.t., 15 min; (c,ii)  $\text{H}_2\text{O}$ , r.t., 5 min; then Conc. HCl, r.t., 5 min; (d,i) oxalyl chloride, DMF, dry DCM, r.t., 20 min; (d,ii) *N,O*-dimethylhydroxylamine hydrochloride,  $\text{K}_2\text{CO}_3$ , dry MeCN, r.t., 30 min; (e) *t*-BuLi, dry THF,  $-78^\circ\text{C}$ , 10 min; (f) 3-bromo-4-pyridinecarboxaldehyde, *p*-toluenesulfonic acid monohydrate, toluene, reflux, 4 h; (g)  $\text{Pd}(\text{dba})_2$ ,  $\text{Ph}_3\text{P}$ , tributyl(1-ethoxyvinyl)stannane, toluene,  $110^\circ\text{C}$ , 10 h; (h) 6 N HCl,  $\text{H}_2\text{O}$ ,  $50^\circ\text{C}$ , 1 h; (i) Xantphos,  $\text{Pd}(\text{OAc})_2$ ,  $\text{Et}_3\text{N}$  in toluene, 2,4,6-trichlorophenyl formate, dry toluene,  $110^\circ\text{C}$ , 10 h; (j) 0.4 M  $\text{NH}_3$  in dioxane,  $80^\circ\text{C}$ , 17 h; (k) benzyl bromides with different substituents, dry MeCN,  $85^\circ\text{C}$ , 1–3 h.

## 2.2. In Vitro Inhibition of AChE Enzyme and Structure-Activity Relationship

The inhibitory potencies of compounds **10a–10s** and **13a–13p** toward AChE were evaluated using the Ellman's assay [23]. Donepezil was used as a positive control. The anti-AChE activities for all target compounds expressed as  $IC_{50}$  values were summarized in Table 1. The results in Table 1 indicated that most of the target compounds exhibited potent inhibitory activities against AChE. Overall, fourteen compounds had better inhibitory activities than positive control donepezil ( $IC_{50} = 12.06$  nM). Among them, compound **10a** ( $IC_{50} = 1.61$  nM) was the most potent compound in the first series of compounds **10a–10s**, showing the best inhibitory activity of all the target compounds. Compound **13b** ( $IC_{50} = 3.54$  nM) was the best compound in the second series of compounds **13a–13p**. Analyzing the results of activity from the perspective of substituents on the benzyl group, it could be found that the substitution of different groups and positions on the benzene ring has a significant differentiation on the inhibitory activity. On the one hand, based on the substituted position in benzene ring, the order of inhibitory potency against AChE was: ortho > meta > para. Furthermore, for the different substituents at the same position, the activity order of the first series of compounds was H > F > Me > Cl > Br > NO<sub>2</sub> > CF<sub>3</sub>, and the activity order of the second series was F > H > Me > Cl > Br > CF<sub>3</sub>; it could be seen that the more appropriate substituents were H (**10a**) or F (**13b**), and the less active substituents were CF<sub>3</sub> (**10s** and **13p**) in these two series, respectively, indicating the order of activity was not much related to the electrical effect of the substituent groups and it may be also related to the steric effect of substituent groups. By analysis of the substituents on the pyridine ring, we found that the first series of compounds **10a–10s** performed better in activity overall. In summary, the above results suggested that the acetyl substitution on the pyridine ring (**10a–10s**) was better than the carbamoyl substitution (**13a–13p**), and the carbonyl moiety may be a key group in the series of skeleton structures. We chose the most potent compound **10a** for further investigations.

**Table 1.** In vitro AChE inhibitory activity of compounds **10a–10s** and **13a–13p**.



Compd.	X	R	$IC_{50}^a$ (nM)		Compd.	X	R	$IC_{50}^a$ (nM)	
			AChE					AChE	
<b>10a</b>	Me	H	1.61 ± 0.02		<b>10s</b>	Me	4-CF <sub>3</sub>	325.94 ± 9.01	
<b>10b</b>	Me	2-F	3.32 ± 0.21		<b>13a</b>	NH <sub>2</sub>	H	8.63 ± 0.06	
<b>10c</b>	Me	3-F	4.03 ± 0.23		<b>13b</b>	NH <sub>2</sub>	2-F	3.54 ± 0.05	
<b>10d</b>	Me	4-F	7.69 ± 0.35		<b>13c</b>	NH <sub>2</sub>	3-F	6.02 ± 0.08	
<b>10e</b>	Me	2-Cl	5.86 ± 0.86		<b>13d</b>	NH <sub>2</sub>	4-F	8.25 ± 0.13	
<b>10f</b>	Me	3-Cl	10.26 ± 1.08		<b>13e</b>	NH <sub>2</sub>	2-Cl	17.58 ± 0.30	
<b>10g</b>	Me	4-Cl	67.32 ± 2.68		<b>13f</b>	NH <sub>2</sub>	3-Cl	26.74 ± 0.28	
<b>10h</b>	Me	2-Br	6.22 ± 0.05		<b>13g</b>	NH <sub>2</sub>	4-Cl	188.34 ± 4.78	
<b>10i</b>	Me	3-Br	10.98 ± 0.82		<b>13h</b>	NH <sub>2</sub>	2-Br	21.71 ± 0.32	
<b>10j</b>	Me	4-Br	75.72 ± 3.18		<b>13i</b>	NH <sub>2</sub>	3-Br	38.14 ± 0.92	
<b>10k</b>	Me	2-Me	4.80 ± 0.26		<b>13j</b>	NH <sub>2</sub>	4-Br	421.76 ± 5.92	
<b>10l</b>	Me	3-Me	6.61 ± 0.81		<b>13k</b>	NH <sub>2</sub>	2-Me	12.14 ± 0.90	
<b>10m</b>	Me	4-Me	54.10 ± 3.22		<b>13l</b>	NH <sub>2</sub>	3-Me	16.26 ± 0.12	
<b>10n</b>	Me	2-NO <sub>2</sub>	13.58 ± 0.72		<b>13m</b>	NH <sub>2</sub>	4-Me	42.47 ± 0.25	
<b>10o</b>	Me	3-NO <sub>2</sub>	22.45 ± 1.25		<b>13n</b>	NH <sub>2</sub>	2-CF <sub>3</sub>	30.71 ± 0.71	
<b>10p</b>	Me	4-NO <sub>2</sub>	128.86 ± 2.68		<b>13o</b>	NH <sub>2</sub>	3-CF <sub>3</sub>	43.05 ± 0.44	
<b>10q</b>	Me	2-CF <sub>3</sub>	18.87 ± 1.16		<b>13p</b>	NH <sub>2</sub>	4-CF <sub>3</sub>	441.18 ± 7.82	
<b>10r</b>	Me	3-CF <sub>3</sub>	25.32 ± 2.20		<b>Donepezil</b>			12.06 ± 0.01	

<sup>a</sup> All values are expressed as mean ± SEM from three independent experiments.

### 2.3. Kinetic Study of AChE Inhibition

In order to analyze the AChE inhibitory mechanism of these compounds, the most potent compound **10a** was selected for kinetic testing. The mechanistic inhibition study of compound **10a** on the AChE was carried out through kinetic parameters such as maximal velocity ( $V_{max}$ ), inhibitory concentration ( $K_i$ ) and Michaelis–Menten dissociation constant ( $K_m$ ). The reciprocal Lineweaver–Burk plot of compound **10a** on AChE demonstrated that as the concentration of inhibitor increased, both slopes and intercepts increased, and the lines generated by compound **10a** with different concentrations eventually converged in the second quadrant (Figure 3). The results in Figure 3 clearly demonstrated that compound **10a** is a mixed-type inhibitor for AChE, suggesting that compound **10a** bound both CAS and PAS of AChE.

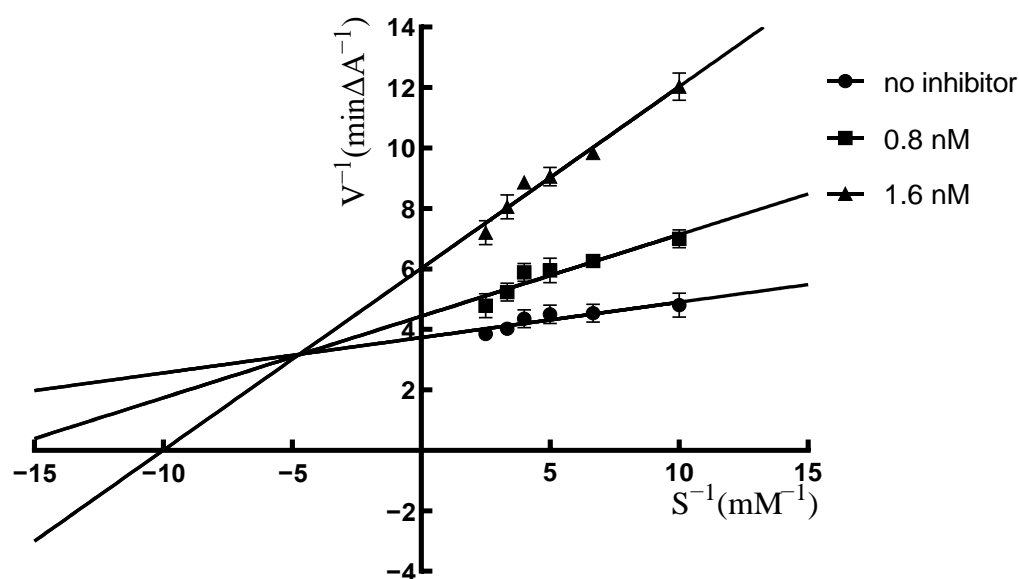


**Figure 3.** Lineweaver–Burk plots generated from the sub-velocity profiles of acetylcholinesterase activity for different substrate concentrations in the absence or presence of **10a** (0, 0.8 and 1.6 nM) (All values are expressed as mean  $\pm$  SEM from three independent experiments).

### 2.4. In Vitro Cytotoxicity of Compounds **10a** and **13b**

To evaluate the cytotoxicity of these new compounds, cell viability was tested on SH-SY5Y cells. The representative compounds **10a** and **13b** in these two series were selected for cytotoxicity. As shown in Figure 4, both compounds **10a** and **13b** did not significantly alter cell viability at concentrations of 10, 25 and 50  $\mu$ M, indicating that compounds **10a** and **13b** had no neurotoxicity up to the concentration at 50  $\mu$ M.

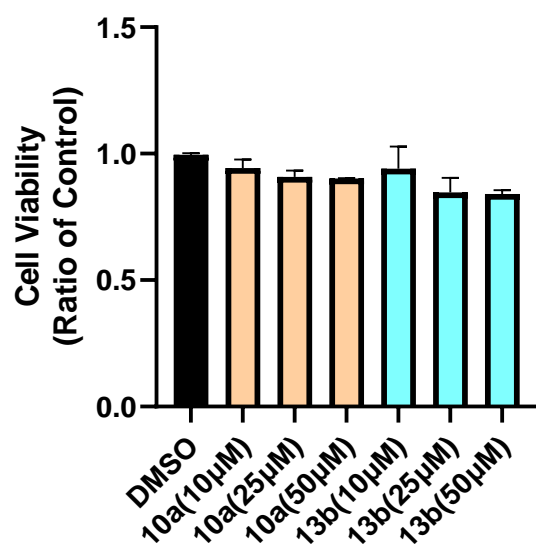


**Figure 4.** Cell viability of compounds **10a** and **13b** on SH-SY5Y cells. All values were expressed as mean  $\pm$  SEM from three independent experiments.

#### 2.5. In Vitro Antioxidant Activity of Compound **10a**

DPPH assay was used to evaluate the free radical scavenging ability of the representative compound **10a**, while Trolox was used as a control [33]. As shown in Table 2, compound **10a** displayed moderate radical scavenging activity ( $31.89\% \pm 3.23\%$  at  $50 \mu\text{M}$ ). The result showed that compound **10a** possessed moderate antioxidant activity at a concentration of  $50 \mu\text{M}$ .

**Table 2.** The antioxidant activity of compound **10a**.

Compound	Concentration	Reduced DPPH <sup>a</sup> (%)
10a	$50 \mu\text{M}$	$31.89 \pm 3.23$
Trolox	$50 \mu\text{M}$	$72.41 \pm 4.23$

<sup>a</sup> All values were expressed as mean  $\pm$  SEM from three independent experiments, the concentration of both compounds **10a** and Trolox are at  $50 \mu\text{M}$ .

#### 2.6. Inhibition of A $\beta$ Self-Aggregation of Compound **10a**

Aggregation of  $\beta$ -amyloid peptide (A $\beta$ ) is one of the main histopathological hallmarks of AD [34]. Therefore, we selected the optimal compound **10a** using a thioflavin T assay to determine the prevention of A $\beta$  aggregation. As shown in Table 3, compound **10a** had a moderate inhibitory effect on the A $\beta$  aggregation, with an inhibitory rate of  $56.95 \pm 2.68\%$  at a concentration of  $25 \mu\text{M}$ . The result showed that compound **10a** exhibited moderate anti-A $\beta$  aggregation efficacy.

**Table 3.** The A $\beta$  aggregation inhibition of compound **10a** and control resveratrol.

Compound	Concentration	A $\beta$ Aggregation Inhibition <sup>a</sup> (%)
10a	$25 \mu\text{M}$	$56.95 \pm 2.68$
Resveratrol	$25 \mu\text{M}$	$83.34 \pm 5.23$

<sup>a</sup> All values were expressed as mean  $\pm$  SEM from three independent experiments.

#### 2.7. Molecular Docking

In order to assess how ligand interacts with enzyme, docking simulations were performed using the Glide program of Schrodinger. The X-ray crystal structure of human AChE (PDB entry 4EY7) was downloaded from PDB. Based on the in vitro inhibitory results, compound **10a** was selected as a typical ligand for the evaluation. The docking results

are shown in Figure 5. The isochromanone fragment was located at the PAS site outside pocket, and the benzyl-substituted pyridine fragment was located at the CAS site inside pocket. Some previous studies showed a proposed H-bonding of donepezil's C=O group with human AChE; however, we did not find the proposed H-bonding of C=O group of compound **10a** with human AChE, but we found that the pharmacophore of compound **10a** based on isochromanone structure of  $\pm$ (XJP-B) could occupy PAS well. Among them, the benzene ring of the isochromanone fragment forms a  $\pi$ - $\pi$  interaction with Trp-286 residue, the pyridine ring forms a  $\pi$ - $\pi$  interaction with Tyr-337 residue, and the benzyl ring formed a  $\pi$ - $\pi$  interaction with Trp-86 residue (brown-dashed line); the acetyl group on the pyridine ring formed a 2.2 Å hydrogen bond with Tyr-124 residue (black-dashed line); the N atom on pyridine ring was connected to Try-337 residue and Trp-86 residue, the two aromatic rings of the radical formed three  $\pi$ -cations interaction (blue-dashed line). All these results indicated that compound **10a** can simultaneously bind to the PAS and CAS of AChE, which is in accordance with the results of the kinetic study.

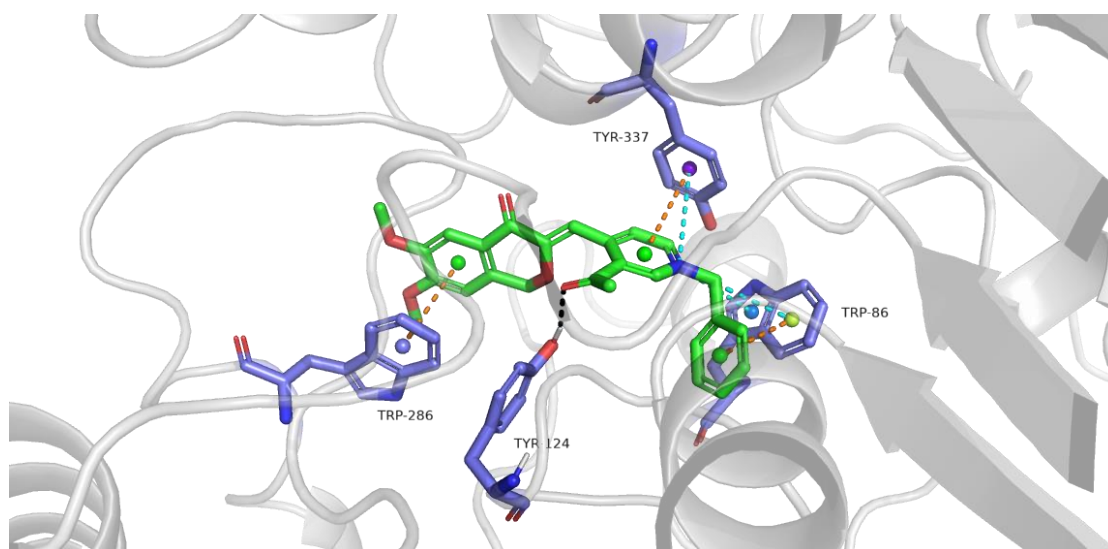


**Figure 5.** Representative compound **10a** interacts with residues in the AChE pocket. The hydrogen bonds of ligand with the target are shown by black-dashed line,  $\pi$ - $\pi$  interaction is shown by brown-dashed line,  $\pi$ -cations interaction is shown by blue-dashed line.

### 2.8. Prediction of Toxicity and Drug-Likeness Properties

To evaluate the drug-likeness characteristics and predict toxicity of the target compounds, blood–brain barrier (BBB) penetration, human intestinal absorption (HIA), caco-2 cells permeability, AMES mutagenesis, and rat acute toxicity were calculated using admet-SAR web-based application tool [35]. Some compounds with better activity were selected for this experiment. As shown in Table 4, according to the predicted values for BBB penetration, all compounds would be able to penetrate into the CNS. However, in the case of HIA and Caco-2 permeability, all compounds performed less well. Compound **10n** with an interposition nitro substitution on the benzyl group showed the only exception to the AMES mutagenicity, which showed potential genotoxicity (“+” sign), indicating that nitro was not a suitable substituent. Overall, the results indicated that these new compounds exhibit good drug-like properties, but there was scope for further improvement.



**Table 4.** ADMET properties and toxicity prediction of selected compounds.

Compd.	BBB Penetration		HIA (%)	Caco-2 <sup>a</sup> Permeability	AMES <sup>b</sup> Mutagenesis	Rat Acute Toxicity
	CNS Activity	%				LD <sub>50</sub> (mol/kg)
10a	+	95	63	-	-	2.74
10b	+	95	78	-	-	2.74
10c	+	95	78	-	-	2.74
10d	+	96	77	-	-	2.73
10e	+	95	63	-	-	2.75
10h	+	95	71	-	-	2.73
10i	+	95	71	-	-	2.73
10k	+	94	63	-	-	2.74
10l	+	95	63	-	-	2.75
10n	+	86	66	-	+	2.71
13a	+	94	70	-	-	2.58
13b	+	95	83	-	-	2.59
13c	+	95	83	-	-	2.59
13d	+	95	83	-	-	2.59
13e	+	94	70	-	-	2.58
13f	+	94	70	-	-	2.58

<sup>a</sup> The values less than 50 are considered as -. <sup>b</sup> The values indicated potential genotoxicity are considered as +.

### 3. Experimental Section

#### 3.1. Chemistry

##### 3.1.1. Materials and Methods

All commercially available chemicals and reagents were analytical grade and used without further purification only if otherwise noted. The <sup>1</sup>H NMR and <sup>13</sup>C NMR were recorded on Bruker-300 spectrometers (Bruker Company, Karlsruhe, Germany) using TMS as an internal standard. High-resolution mass spectrometry was accomplished on an Agilent 1100-LC-MSD-Trap/SL mass spectrometer (Agilent Technologies Inc., Santa Clara, CA, USA). Huanghai HSGF 254 silica gel plates (Yantai, China) were used for TLC. Silica gel 60 H (200–300 mesh), general chromatography was performed manufactured by Qingdao Haiyang Chemical Group Co., Ltd. (Qingdao, China).

##### 3.1.2. Synthesis of (2-Bromo-4,5-dimethoxyphenyl)methanol (2)

To a solution of 2-bromo-4,5-dimethoxybenzaldehyde (1) (81.61 mmol, 1 eq) in 100 mL methanol, sodium borohydride (40.80 mmol, 0.5 eq) was slowly added at 0 °C and the mixture was stirred at the same temperature. After the completion of the reaction was detected by TLC, crushed ice was added into the mixture and stirred for another 1 h. After filtration, the filtrate was washed with cold water and collected as a white solid [32].

##### 3.1.3. Synthesis of Tert-butyl 2-((2-bromo-4,5-dimethoxybenzyl)oxy)acetate (3)

To a solution of (2-bromo-4,5-dimethoxyphenyl)methanol (2) (40.47 mmol, 1 eq) in 100 mL toluene, *tert*-butyl bromoacetate (48.57 mmol, 1.2 eq), fresh 40% KOH aqueous solution (100 mL) and the catalytic amount of tetrabutylammonium bromide were added successively, stirred at 50 °C for 1 h. After the completion of the reaction was detected by TLC, the mixture was extracted with ethyl acetate (3 × 200 mL). The combined organic layers were washed with brine (200 mL) and dried over anhydrous Na<sub>2</sub>SO<sub>4</sub>. The organic layers were removed in vacuo to give crude colorless oil 3 [32].

##### 3.1.4. Synthesis of 2-((2-Bromo-4,5-dimethoxybenzyl)oxy)acetic Acid (4)

To a solution of *tert*-butyl 2-((2-bromo-4,5-dimethoxybenzyl)oxy)acetate (3) in 100 mL methanol, a solution of sodium methanol (101.04 mmol, 2.5 eq) in methanol was slowly added; the mixture was stirred at room temperature for about 15 min, and an appropriate amount of H<sub>2</sub>O was slowly added to the mixture with vigorous stirring for 5 min. After the reaction was completed, the solvent was concentrated and the aqueous layer was extracted

with ethyl acetate (3 × 200 mL). The pH of the aqueous layer was adjusted to 2 by slowly adding concentrated hydrochloric, and then the aqueous layer was extracted three times with ethyl acetate. The combined organic layers were washed with brine (100 mL) and dried over anhydrous Na<sub>2</sub>SO<sub>4</sub>. The organic layers were removed in vacuo to give crude white solid 4 [32].

### 3.1.5. Synthesis of 2-((2-Bromo-4,5-dimethoxybenzyl)oxy)-*n*-methoxy-*n*-methylacetamide (5)

Intermediate 2-((2-bromo-4,5-dimethoxybenzyl)oxy)acetic acid (4) (32.77 mmol, 1 eq) was dissolved in dry DCM (50 mL), oxalyl chloride (98.32 mmol, 3 eq) and 1–2 drops of DMF solution were slowly added and the reaction stirred 20 min at room temperature. The organic layers were removed in vacuo to give crude acyl chloride intermediate. In another flask, 50 mL of dry acetonitrile was used as solvent. *N,O*-dimethylhydroxylamine hydrochloride (36.05 mmol, 1.1 eq) and anhydrous potassium carbonate (81.93 mmol, 2.5 eq) were added sequentially and mixed well. After the reaction completed, the mixture was filtered to remove the residual insoluble matter, and the filtrate was concentrated and purified by column chromatography to give a white solid 5 [32].

### 3.1.6. Synthesis of 6,7-Dimethoxyisochroman-4-one (6)

Intermediate 2-((2-bromo-4,5-dimethoxybenzyl)oxy)-*N*-methoxy-*N*-methylacetamide 5 (14.36 mmol, 1 eq) was dissolved in anhydrous THF under an N<sub>2</sub> atmosphere and placed at a low temperature of −78 °C. A solution of 1.3 M *tert*-butyllithium (35.90 mmol, 2.5 eq) in *n*-pentane was added and the mixture was stirred for another 10 min. At the end of the reaction, a saturated aqueous ammonium chloride solution was added to quench the reaction and the mixture was brought to room temperature. The residue was extracted with ethyl acetate (EA) (3 × 200 mL), the organic layers were combined, washed with brine, dried over anhydrous Na<sub>2</sub>SO<sub>4</sub>, and the organic layers were concentrated and purified by column chromatography to give pale yellow solid 6. <sup>1</sup>H NMR (300 MHz, CDCl<sub>3</sub>) δ 7.50 (s, 1H), 6.64 (s, 1H), 4.85 (s, 2H), 4.33 (s, 2H), 3.95 (d, *J* = 6.7 Hz, 6H). <sup>13</sup>C NMR (75 MHz, CDCl<sub>3</sub>) δ 196.7, 154.0, 149.1, 127.5, 126.3, 118.8, 109.3, 81.1, 72.7, 56.2, 56.1. MS (ESI) *m/z*: 209.18 [M + H]<sup>+</sup>.

### 3.1.7. Synthesis of (Z)-3-((3-Bromopyridin-4-yl)methylene)-6,7-dimethoxyisochroman-4-one (7)

To a solution of Intermediate 6 (4.80 mmol, 1 eq) in dry toluene, 3-bromopyridine-4-aldehyde (7.20 mmol, 1.5 eq) and *p*-toluenesulfonic acid monohydrate (7.20 mmol, 1.5 eq) were added sequentially and the mixture stirred at reflux for 4 h. At the end of the reaction, the reaction system was cooled to room temperature, and the pH was adjusted to 8 by adding saturated sodium bicarbonate. The mixture was extracted with dichloromethane (3 × 200 mL). The organic layer was washed with brine and dried over anhydrous Na<sub>2</sub>SO<sub>4</sub>, and purified by column chromatography to give yellow solid 7. <sup>1</sup>H NMR (300 MHz, CDCl<sub>3</sub>) δ 8.76 (s, 1H), 8.50 (d, *J* = 5.1 Hz, 1H), 8.06 (d, *J* = 5.0 Hz, 1H), 7.58 (s, 1H), 7.25 (s, 1H), 6.66 (s, 1H), 5.29 (s, 2H), 3.99 (d, *J* = 4.8 Hz, 6H). <sup>13</sup>C NMR (75 MHz, CDCl<sub>3</sub>) δ 178.5, 157.5, 156.0, 149.6, 149.6, 148.2, 147.1, 132.5, 125.7, 118.6, 118.6, 118.4, 106.2, 102.6, 70.5, 56.1, 56.0. MS (ESI) *m/z*: 376.41 [M + H]<sup>+</sup>.

### 3.1.8. Synthesis of (Z)-3-((3-(1-Ethoxyvinyl)pyridine-4-yl)methylene)-6,7-dimethoxyisochroman-4-one (8)

To a solution of intermediate 7 (3.46 mmol, 1 eq) in dry toluene at nitrogen atmosphere, *p*-(diaziridine acetonide)palladium (0.05 mmol, 0.04 eq), tributyl(1-ethoxyethylene)tin (1.37 mmol, 1.2 eq) and triphenylphosphine (0.09 mmol, 0.08 eq) were added sequentially and stirred at reflux for 10 h, then brought to room temperature. After filtration, the filtrate was concentrated and purified by column chromatography to give yellow solid, which was further recrystallized by dichloromethane/petroleum ether to give intermediate 8.

### 3.1.9. Synthesis of (Z)-3-((3-Acetylpyridin-4-yl)methylene)-6,7-dimethoxyisochroman-4-one (**9**)

Intermediate **8** dissolved in 6 N aqueous HCl and stirred for 1 h at 50 °C. After the reaction completed, the hydrochloric acid was neutralized by adding saturated sodium bicarbonate solution and the organic layer was extracted with dichloromethane. The organic layer was washed with saturated salt water, dried over anhydrous sodium sulphate, concentrated and recrystallized using a mixture of dichloromethane/petroleum to give yellow solid **9**.

### 3.1.10. Synthesis of 2,4,6-Trichlorophenyl 4-((5,6-dimethoxy-1-oxo-2,3-dihydro-1H-inden-2-yl)methyl)nicotinate (**11**)

To a solution of intermediate **7** (3.46 mmol, 1 eq) in dry toluene at nitrogen atmosphere, xantphos (0.34 mmol, 0.1 eq), palladium acetate (0.17 mmol, 0.05 eq) and triethylamine (6.91 mmol, 2 eq) were added sequentially and stirred at 100 °C for 5 min, then brought to room temperature. 2,4,6-Trichlorophenyl ester (5.18 mmol, 1.5 eq) was added to the mixture. After filtration, the filtrate was concentrated and purified by column chromatography to give a yellow solid, which was further recrystallized by dichloromethane/petroleum to give intermediate **11**.

### 3.1.11. Synthesis of (Z)-4-((6,7-Dimethoxy-4-oxoisochroman-3-ylidene)methyl)nicotinamide (**12**)

Intermediate **11** was added into 0.4 M ammonia (17.3 mmol, 5 eq) in dioxane solution in a pressure resistant sealing tube. The mixture was stirred at 80 °C for 17 h. The solvent was removed in vacuo, and was further recrystallized by ethyl acetate to give intermediate **12**.

### 3.1.12. Synthesis of Target Compounds **10a–10s**

To a solution of intermediate **9** in dry acetonitrile, benzyl bromide with different substituents (0.71 mmol, 3 eq) was added and stirred for 1–3 h at 85 °C. The solvent was removed under reduced pressure and recrystallized by ethyl acetate to give **10a–10s**.

#### (Z)-3-Acetyl-1-benzyl-4-((6,7-dimethoxy-4-oxoisochroman-3-ylidene)methyl)pyridin-1-ium bromide (**10a**)

Yellow solid, 90.5% yield. <sup>1</sup>H NMR (300 MHz, DMSO-*d*<sub>6</sub>) δ 9.75 (s, 1H), 9.10 (d, *J* = 6.4 Hz, 1H), 8.69 (d, *J* = 6.8 Hz, 1H), 7.60 (s, 2H), 7.51–7.36 (m, 4H), 7.31 (s, 1H), 7.12 (s, 1H), 5.89 (s, 2H), 5.50 (s, 2H), 3.88 (d, *J* = 14.1 Hz, 6H), 2.76 (s, 3H). <sup>13</sup>C NMR (75 MHz, DMSO-*d*<sub>6</sub>) δ 197.8, 176.9, 156.9, 155.5, 150.9, 149.7, 148.9, 145.3, 144.7, 134.9, 129.7, 129.4, 128.1, 127.1, 125.8, 125.2, 121.2, 116.4, 107.6, 105.0, 103.5, 67.6, 62.9, 56.8, 56.2, 30.7. HR-MS (ESI) *m/z*: calcd for C<sub>26</sub>H<sub>24</sub>NO<sub>5</sub> [M]<sup>+</sup> 430.1649, found 430.1649.

#### (Z)-3-Acetyl-4-((6,7-dimethoxy-4-oxoisochroman-3-ylidene)methyl)-1-(2-fluorobenzyl)pyridin-1-ium Bromide (**10b**)

Yellow solid, 85.3% yield. <sup>1</sup>H NMR (300 MHz, DMSO-*d*<sub>6</sub>) δ 9.62 (s, 1H), 9.04 (d, *J* = 6.8 Hz, 1H), 8.77 (d, *J* = 6.7 Hz, 1H), 7.65 (dd, *J* = 13.7, 6.2 Hz, 1H), 7.61–7.53 (m, 1H), 7.47 (s, 1H), 7.41 (d, *J* = 10.0 Hz, 1H), 7.36 (d, *J* = 4.2 Hz, 2H), 7.17 (s, 1H), 6.00 (s, 2H), 5.56 (s, 2H), 3.95 (s, 3H), 3.90 (s, 3H), 2.77 (s, 3H). <sup>13</sup>C NMR (75 MHz, DMSO-*d*<sub>6</sub>) δ 197.7, 176.8, 162.2, 159.7, 156.6, 155.5, 149.7, 149.2, 145.9, 145.5, 135.3, 135.1, 132.5, 131.8, 128.0, 125.7, 121.8, 121.2, 116.4, 107.6, 103.3, 67.6, 57.6, 56.8, 56.2, 30.6. HR-MS (ESI) *m/z*: calcd for C<sub>27</sub>H<sub>26</sub>FNO<sub>6</sub> [M + CH<sub>3</sub>OH]<sup>+</sup> 448.1817, found 480.1823.

#### (Z)-3-Acetyl-4-((6,7-dimethoxy-4-oxoisochroman-3-ylidene)methyl)-1-(3-fluorobenzyl)pyridin-1-ium Bromide (**10c**)

Yellow solid, 86.4% yield. <sup>1</sup>H NMR (300 MHz, DMSO-*d*<sub>6</sub>) δ 9.69 (s, 1H), 9.11 (d, *J* = 6.8 Hz, 1H), 8.73 (d, *J* = 6.7 Hz, 1H), 7.60–7.51 (m, 2H), 7.50–7.43 (m, 2H), 7.37–7.27 (m, 2H), 7.15 (s, 1H), 5.91 (s, 2H), 5.53 (s, 2H), 3.93 (s, 3H), 3.88 (s, 3H), 2.77 (s, 3H). <sup>13</sup>C NMR (75 MHz, DMSO-*d*<sub>6</sub>) δ 197.8, 176.8, 164.3, 161.0, 156.5, 155.5, 149.7, 149.1, 146.0, 145.3, 137.2, 135.1, 131.7, 128.1, 125.6, 121.2, 116.6, 116.3, 107.9, 107.6, 103.4, 67.6, 62.1, 56.8, 56.2, 30.6. HR-MS (ESI) *m/z*: calcd for C<sub>27</sub>H<sub>26</sub>FNO<sub>6</sub> [M + CH<sub>3</sub>OH]<sup>+</sup> 480.1817, found 480.1819.

(Z)-3-Acetyl-4-((6,7-dimethoxy-4-oxoisochroman-3-ylidene)methyl)-1-(4-fluorobenzyl)pyridin-1-ium Bromide (**10d**)

Yellow solid, 88.3% yield.  $^1\text{H}$  NMR (300 MHz, DMSO- $d_6$ )  $\delta$  9.70 (s, 1H), 9.11 (d,  $J = 6.7$  Hz, 1H), 8.72 (d,  $J = 6.7$  Hz, 1H), 7.75 (dd,  $J = 8.2, 5.7$  Hz, 2H), 7.45 (s, 1H), 7.35 (dd,  $J = 10.7, 6.8$  Hz, 3H), 7.16 (s, 1H), 5.90 (s, 2H), 5.53 (s, 2H), 3.94 (s, 3H), 3.89 (s, 3H), 2.78 (s, 3H).  $^{13}\text{C}$  NMR (75 MHz, DMSO- $d_6$ )  $\delta$  197.8, 176.8, 164.7, 161.4, 156.4, 155.5, 149.7, 148.9, 145.7, 145.1, 135.2, 135.1, 132.1, 131.0, 128.1, 121.2, 116.7, 116.4, 107.9, 107.5, 103.4, 67.5, 62.0, 56.8, 56.2, 30.6. HR-MS (ESI)  $m/z$ : calcd for  $\text{C}_{27}\text{H}_{26}\text{FNO}_6$  [ $\text{M} + \text{CH}_3\text{OH}$ ] $^+$  480.1817, found 480.1822.

(Z)-3-Acetyl-1-(2-chlorobenzyl)-4-((6,7-dimethoxy-4-oxoisochroman-3-ylidene)methyl)pyridin-1-ium Bromide (**10e**)

Brown solid, 87.9% yield.  $^1\text{H}$  NMR (300 MHz, DMSO- $d_6$ )  $\delta$  9.60 (s, 1H), 8.97 (d,  $J = 6.8$  Hz, 1H), 8.77 (d,  $J = 6.8$  Hz, 1H), 7.66 (d,  $J = 7.8$  Hz, 1H), 7.58–7.52 (m, 1H), 7.49 (d,  $J = 6.4$  Hz, 2H), 7.46 (s, 1H), 7.38 (s, 1H), 7.16 (s, 1H), 6.02 (s, 2H), 5.55 (s, 2H), 3.94 (s, 3H), 3.89 (s, 3H), 2.75 (s, 3H).  $^{13}\text{C}$  NMR (75 MHz, DMSO- $d_6$ )  $\delta$  197.8, 176.8, 156.8, 155.5, 149.7, 149.3, 146.3, 145.6, 135.1, 133.4, 132.1, 131.7, 131.4, 130.5, 128.6, 127.9, 121.2, 112.9, 107.9, 107.6, 103.2, 67.6, 60.9, 56.8, 56.2, 30.6. HR-MS (ESI)  $m/z$ : calcd for  $\text{C}_{26}\text{H}_{23}\text{ClNO}_5$  [ $\text{M}$ ] $^+$  464.1259, found 464.1254.

(Z)-3-Acetyl-1-(3-chlorobenzyl)-4-((6,7-dimethoxy-4-oxoisochroman-3-ylidene)methyl)pyridin-1-ium Bromide (**10f**)

Yellow solid, 90.0% yield.  $^1\text{H}$  NMR (300 MHz, DMSO- $d_6$ )  $\delta$  9.70 (s, 1H), 9.11 (d,  $J = 6.8$  Hz, 1H), 8.73 (d,  $J = 6.7$  Hz, 1H), 7.80 (s, 1H), 7.61 (s, 1H), 7.55 (s, 2H), 7.45 (s, 1H), 7.35 (s, 1H), 7.16 (s, 1H), 5.90 (s, 2H), 5.54 (s, 2H), 3.93 (s, 3H), 3.89 (s, 3H), 2.78 (s, 3H).  $^{13}\text{C}$  NMR (75 MHz, DMSO- $d_6$ )  $\delta$  197.8, 176.8, 156.5, 155.5, 149.7, 149.1, 146.0, 145.2, 136.9, 135.2, 135.1, 134.1, 131.5, 129.8, 129.4, 128.2, 128.1, 121.2, 107.9, 107.5, 103.4, 67.5, 62.0, 56.8, 56.2, 30.7. HR-MS (ESI)  $m/z$ : calcd for  $\text{C}_{26}\text{H}_{23}\text{ClNO}_5$  [ $\text{M}$ ] $^+$  464.1259, found 464.1257.

(Z)-3-Acetyl-1-(4-chlorobenzyl)-4-((6,7-dimethoxy-4-oxoisochroman-3-ylidene)methyl)pyridin-1-ium Bromide (**10g**)

Brown solid, 90.3% yield.  $^1\text{H}$  NMR (300 MHz, DMSO- $d_6$ )  $\delta$  9.67 (s, 1H), 9.07 (d,  $J = 6.6$  Hz, 1H), 8.70 (d,  $J = 6.8$  Hz, 1H), 7.66 (d,  $J = 8.5$  Hz, 2H), 7.55 (d,  $J = 8.5$  Hz, 2H), 7.42 (s, 1H), 7.32 (s, 1H), 7.13 (s, 1H), 5.88 (s, 2H), 5.51 (s, 2H), 3.91 (s, 3H), 3.86 (s, 3H), 2.75 (s, 3H).  $^{13}\text{C}$  NMR (75 MHz, DMSO- $d_6$ )  $\delta$  197.8, 176.8, 156.4, 155.5, 149.7, 149.0, 145.9, 145.2, 135.2, 135.1, 134.6, 133.6, 131.5, 131.5, 129.6, 129.6, 128.1, 121.2, 107.9, 107.6, 103.4, 67.6, 62.0, 56.8, 56.2, 30.7. HR-MS (ESI)  $m/z$ : calcd for  $\text{C}_{26}\text{H}_{23}\text{ClNO}_5$  [ $\text{M}$ ] $^+$  464.1259, found 464.1247.

(Z)-3-Acetyl-1-(2-bromobenzyl)-4-((6,7-dimethoxy-4-oxoisochroman-3-ylidene)methyl)pyridin-1-ium Bromide (**10h**)

Brown solid, 88.3% yield.  $^1\text{H}$  NMR (300 MHz, DMSO- $d_6$ )  $\delta$  9.59 (s, 1H), 8.93 (d,  $J = 7.0$  Hz, 1H), 8.76 (d,  $J = 6.8$  Hz, 1H), 7.80 (d,  $J = 7.9$  Hz, 1H), 7.54–7.47 (m, 1H), 7.47–7.41 (m, 2H), 7.39–7.31 (m, 2H), 7.14 (s, 1H), 5.96 (s, 2H), 5.54 (s, 2H), 3.92 (s, 3H), 3.87 (s, 3H), 2.73 (s, 3H).  $^{13}\text{C}$  NMR (75 MHz, DMSO- $d_6$ )  $\delta$  197.7, 176.8, 156.8, 156.1, 155.5, 154.9, 153.4, 149.7, 149.4, 135.1, 135.0, 133.8, 131.3, 130.1, 129.1, 127.9, 123.6, 121.2, 107.9, 107.6, 103.2, 68.5, 63.1, 56.8, 56.2, 30.6. HR-MS (ESI)  $m/z$ : calcd for  $\text{C}_{26}\text{H}_{23}\text{BrNO}_5$  [ $\text{M}$ ] $^+$  508.0754, found 508.0761.

(Z)-3-Acetyl-1-(3-bromobenzyl)-4-((6,7-dimethoxy-4-oxoisochroman-3-ylidene)methyl)pyridin-1-ium Bromide (**10i**)

Yellow solid, 80.5% yield.  $^1\text{H}$  NMR (300 MHz, DMSO- $d_6$ )  $\delta$  9.65 (s, 1H), 9.08 (d,  $J = 6.8$  Hz, 1H), 8.71 (d,  $J = 6.8$  Hz, 1H), 7.90 (s, 1H), 7.69–7.59 (m, 2H), 7.48–7.40 (m, 2H), 7.33 (s, 1H), 7.13 (s, 1H), 5.86 (s, 2H), 5.51 (s, 2H), 3.91 (s, 3H), 3.86 (s, 3H), 2.75 (s, 3H).  $^{13}\text{C}$  NMR (75 MHz, DMSO- $d_6$ )  $\delta$  197.8, 176.8, 156.5, 155.5, 149.7, 149.1, 146.0, 145.2, 137.1, 135.2, 135.1, 132.7, 132.3, 131.8, 128.6, 128.1, 122.7, 121.2, 107.9, 107.6, 103.4, 67.6, 62.0, 56.8, 56.2, 30.7. HR-MS (ESI)  $m/z$ : calcd for  $\text{C}_{27}\text{H}_{26}\text{BrNO}_6$  [ $\text{M} + \text{CH}_3\text{OH}$ ] $^+$  540.1016, found 540.1018.

(Z)-3-Acetyl-1-(4-bromobenzyl)-4-((6,7-dimethoxy-4-oxoisochroman-3-ylidene)methyl)pyridin-1-ium Bromide (**10j**)

Brown solid, 88.7% yield.  $^1\text{H}$  NMR (300 MHz,  $\text{DMSO-}d_6$ )  $\delta$  9.65 (s, 1H), 9.08 (d,  $J = 6.5$  Hz, 1H), 8.72 (d,  $J = 6.5$  Hz, 1H), 7.72 (d,  $J = 7.3$  Hz, 2H), 7.60 (d,  $J = 7.8$  Hz, 2H), 7.46 (s, 1H), 7.35 (s, 1H), 7.15 (s, 1H), 5.87 (s, 2H), 5.53 (s, 2H), 3.94 (s, 3H), 3.89 (s, 4H), 2.77 (s, 3H).  $^{13}\text{C}$  NMR (75 MHz,  $\text{DMSO-}d_6$ )  $\delta$  197.8, 176.8, 156.4, 155.5, 149.7, 149.0, 145.9, 145.2, 135.2, 135.1, 134.0, 132.6, 132.6, 131.7, 131.7, 128.1, 123.3, 121.2, 107.9, 107.6, 103.4, 67.5, 62.1, 56.8, 56.2, 30.6. HR-MS (ESI)  $m/z$ : calcd for  $\text{C}_{26}\text{H}_{23}\text{BrNO}_5$   $[\text{M}]^+$  508.0754, found 508.0767.

(Z)-3-Acetyl-4-((6,7-dimethoxy-4-oxoisochroman-3-ylidene)methyl)-1-(2-methylbenzyl)pyridin-1-ium Bromide (**10j**)

Brown solid, 84.9% yield.  $^1\text{H}$  NMR (300 MHz,  $\text{DMSO-}d_6$ )  $\delta$  9.59 (s, 1H), 8.88 (d,  $J = 6.8$  Hz, 1H), 8.76 (d,  $J = 6.7$  Hz, 1H), 7.46 (s, 1H), 7.39 (d,  $J = 6.5$  Hz, 3H), 7.32 (t,  $J = 6.9$  Hz, 1H), 7.24–7.14 (m, 2H), 5.94 (s, 2H), 5.54 (s, 2H), 3.94 (s, 3H), 3.89 (s, 3H), 2.76 (s, 3H), 2.39 (s, 3H).  $^{13}\text{C}$  NMR (75 MHz,  $\text{DMSO-}d_6$ )  $\delta$  197.8, 176.8, 156.5, 155.5, 149.7, 149.0, 146.1, 145.3, 137.3, 135.1, 135.1, 132.8, 131.3, 129.7, 129.3, 128.0, 127.1, 121.2, 107.8, 107.6, 103.3, 67.6, 61.2, 56.8, 56.2, 30.7, 19.4. HR-MS (ESI)  $m/z$ : calcd for  $\text{C}_{28}\text{H}_{29}\text{NO}_6$   $[\text{M} + \text{CH}_3\text{OH}]^+$  476.2068, found 476.2076.

(Z)-3-Acetyl-4-((6,7-dimethoxy-4-oxoisochroman-3-ylidene)methyl)-1-(3-methylbenzyl)pyridin-1-ium Bromide (**10l**)

Yellow solid, 85.4% yield.  $^1\text{H}$  NMR (300 MHz,  $\text{DMSO-}d_6$ )  $\delta$  9.69 (s, 1H), 9.09 (d,  $J = 6.8$  Hz, 1H), 8.73 (d,  $J = 6.7$  Hz, 1H), 7.48–7.38 (m, 4H), 7.35 (d,  $J = 4.0$  Hz, 1H), 7.29 (d,  $J = 6.8$  Hz, 1H), 7.16 (s, 1H), 5.83 (d,  $J = 17.7$  Hz, 2H), 5.53 (s, 2H), 3.94 (s, 3H), 3.89 (s, 3H), 2.79 (s, 3H), 2.36 (s, 3H).  $^{13}\text{C}$  NMR (75 MHz,  $\text{DMSO-}d_6$ )  $\delta$  197.8, 176.8, 156.4, 155.5, 149.6, 148.9, 145.7, 145.2, 139.0, 135.2, 135.1, 134.6, 130.4, 129.9, 129.6, 128.0, 126.4, 121.2, 107.9, 107.6, 103.4, 67.5, 62.9, 56.8, 56.2, 30.7, 21.4. HR-MS (ESI)  $m/z$ : calcd for  $\text{C}_{28}\text{H}_{29}\text{NO}_6$   $[\text{M} + \text{CH}_3\text{OH}]^+$  476.2068, found 476.2076.

(Z)-3-Acetyl-4-((6,7-dimethoxy-4-oxoisochroman-3-ylidene)methyl)-1-(4-methylbenzyl)pyridin-1-ium Bromide (**10m**)

Yellow solid, 89.9% yield.  $^1\text{H}$  NMR (300 MHz,  $\text{DMSO-}d_6$ )  $\delta$  9.67 (s, 1H), 9.08 (d,  $J = 6.9$  Hz, 1H), 8.71 (d,  $J = 6.7$  Hz, 1H), 7.54 (d,  $J = 7.9$  Hz, 2H), 7.45 (s, 1H), 7.38–7.22 (m, 3H), 7.16 (s, 1H), 5.84 (s, 2H), 5.53 (s, 2H), 3.94 (s, 3H), 3.89 (s, 3H), 2.78 (s, 3H), 2.35 (s, 3H).  $^{13}\text{C}$  NMR (75 MHz,  $\text{DMSO-}d_6$ )  $\delta$  197.8, 176.8, 156.3, 155.5, 149.6, 148.9, 145.6, 145.1, 139.4, 135.2, 135.1, 131.8, 130.2, 130.2, 129.4, 129.4, 128.1, 121.2, 107.9, 107.5, 103.5, 67.5, 62.7, 56.8, 56.2, 30.7, 21.2. HR-MS (ESI)  $m/z$ : calcd for  $\text{C}_{28}\text{H}_{29}\text{NO}_6$   $[\text{M} + \text{CH}_3\text{OH}]^+$  476.2068, found 476.2075.

(Z)-3-Acetyl-4-((6,7-dimethoxy-4-oxoisochroman-3-ylidene)methyl)-1-(2-nitrobenzyl)pyridin-1-ium Bromide (**10n**)

Yellow solid, 89.2% yield.  $^1\text{H}$  NMR (300 MHz,  $\text{DMSO-}d_6$ )  $\delta$  9.59 (s, 1H), 9.01 (d,  $J = 7.0$  Hz, 1H), 8.82 (d,  $J = 6.7$  Hz, 1H), 8.32 (d,  $J = 7.2$  Hz, 1H), 7.85 (q,  $J = 6.7$  Hz, 1H), 7.82–7.72 (m, 1H), 7.45 (d,  $J = 12.7$  Hz, 2H), 7.27 (d,  $J = 7.3$  Hz, 1H), 7.18 (s, 1H), 6.27 (s, 2H), 5.58 (s, 2H), 3.95 (s, 3H), 3.90 (s, 3H), 2.74 (s, 3H).  $^{13}\text{C}$  NMR (75 MHz,  $\text{DMSO-}d_6$ )  $\delta$  197.7, 176.8, 156.8, 155.5, 149.7, 149.5, 147.9, 146.8, 145.9, 135.4, 135.1, 135.0, 130.8, 130.5, 129.9, 128.0, 126.0, 121.2, 107.9, 107.6, 103.3, 67.6, 60.5, 56.8, 56.2, 30.4. HR-MS (ESI)  $m/z$ : calcd for  $\text{C}_{27}\text{H}_{26}\text{N}_2\text{O}_8$   $[\text{M} + \text{CH}_3\text{OH}]^+$  507.1762, found 507.1769.

(Z)-3-Acetyl-4-((6,7-dimethoxy-4-oxoisochroman-3-ylidene)methyl)-1-(3-nitrobenzyl)pyridin-1-ium Bromide (**10o**)

Yellow solid, 87.3% yield.  $^1\text{H}$  NMR (300 MHz,  $\text{DMSO-}d_6$ )  $\delta$  9.73 (s, 1H), 9.17 (d,  $J = 6.8$  Hz, 1H), 8.74 (d,  $J = 6.7$  Hz, 1H), 8.63 (s, 1H), 8.34 (d,  $J = 8.2$  Hz, 1H), 8.13 (d,  $J = 7.7$  Hz, 1H), 7.81 (t,  $J = 8.0$  Hz, 1H), 7.45 (s, 1H), 7.35 (s, 1H), 7.16 (s, 1H), 6.05 (s, 2H), 5.54 (s, 2H), 3.94 (s, 3H), 3.89 (s, 3H), 2.78 (s, 3H).  $^{13}\text{C}$  NMR (75 MHz,  $\text{DMSO-}d_6$ )  $\delta$  197.8, 176.8, 156.5, 155.5, 149.7, 149.1, 148.5, 146.1, 145.3, 136.4, 136.4, 135.2, 135.1, 131.2, 128.1, 124.9, 124.7, 121.2, 107.8, 107.6, 103.4, 67.6, 61.7, 56.8, 56.2, 30.7. HR-MS (ESI)  $m/z$ : calcd for  $\text{C}_{27}\text{H}_{26}\text{N}_2\text{O}_8$   $[\text{M} + \text{CH}_3\text{OH}]^+$  507.1762, found 507.1768.

(Z)-3-Acetyl-4-((6,7-dimethoxy-4-oxoisochroman-3-ylidene)methyl)-1-(4-nitrobenzyl)pyridin-1-ium Bromide (**10p**)

Brown solid, 91.0% yield.  $^1\text{H}$  NMR (300 MHz,  $\text{DMSO-}d_6$ )  $\delta$  9.69 (s, 1H), 9.12 (d,  $J = 6.9$  Hz, 1H), 8.76 (d,  $J = 6.7$  Hz, 1H), 8.35 (d,  $J = 8.6$  Hz, 2H), 7.86 (d,  $J = 8.6$  Hz, 2H), 7.46 (s, 1H), 7.37 (s, 1H), 7.16 (s, 1H), 6.06 (s, 2H), 5.55 (s, 2H), 3.94 (s, 3H), 3.89 (s, 3H), 2.77 (s, 3H).  $^{13}\text{C}$  NMR (75 MHz,  $\text{DMSO-}d_6$ )  $\delta$  197.7, 176.8, 156.6, 155.5, 149.7, 149.3, 148.3, 146.22, 145.5, 141.7, 135.2, 135.1, 130.6, 130.6, 128.1, 124.6, 124.6, 121.2, 107.9, 107.5, 103.3, 67.6, 61.8, 56.8, 56.2, 30.6. HR-MS (ESI)  $m/z$ : calcd for  $\text{C}_{27}\text{H}_{26}\text{N}_2\text{O}_8$  [ $\text{M} + \text{CH}_3\text{OH}$ ] $^+$  507.1762, found 507.1771.

(Z)-3-Acetyl-4-((6,7-dimethoxy-4-oxoisochroman-3-ylidene)methyl)-1-(2-(trifluoromethyl)benzyl)pyridin-1-ium Bromide (**10q**)

Yellow solid, 90.9% yield.  $^1\text{H}$  NMR (300 MHz,  $\text{DMSO-}d_6$ )  $\delta$  9.57 (s, 1H), 8.92 (d,  $J = 7.0$  Hz, 1H), 8.77 (d,  $J = 6.8$  Hz, 1H), 7.94 (d,  $J = 7.0$  Hz, 1H), 7.81–7.73 (m, 1H), 7.70 (t,  $J = 7.5$  Hz, 1H), 7.44 (s, 1H), 7.38 (s, 1H), 7.26 (d,  $J = 7.3$  Hz, 1H), 7.14 (s, 1H), 6.12 (s, 2H), 5.55 (s, 2H), 3.92 (s, 3H), 3.87 (s, 3H), 2.73 (s, 3H).  $^{13}\text{C}$  NMR (75 MHz,  $\text{DMSO-}d_6$ )  $\delta$  197.8, 176.8, 156.9, 155.5, 149.7, 149.5, 146.7, 145.9, 135.1, 135.1, 134.1, 132.2, 130.4, 130.2, 128.0, 127.3, 126.9, 126.3, 121.2, 107.9, 107.6, 103.1, 67.6, 59.8, 56.8, 56.2, 30.6. HR-MS (ESI)  $m/z$ : calcd for  $\text{C}_{28}\text{H}_{26}\text{F}_3\text{NO}_6$  [ $\text{M} + \text{CH}_3\text{OH}$ ] $^+$  530.1785, found 530.1784.

(Z)-3-Acetyl-4-((6,7-dimethoxy-4-oxoisochroman-3-ylidene)methyl)-1-(3-(trifluoromethyl)benzyl)pyridin-1-ium Bromide (**10r**)

Yellow solid, 87.9% yield.  $^1\text{H}$  NMR (300 MHz,  $\text{DMSO-}d_6$ )  $\delta$  9.73 (s, 1H), 9.14 (d,  $J = 6.5$  Hz, 1H), 8.75 (d,  $J = 5.1$  Hz, 1H), 8.13 (s, 1H), 7.95 (d,  $J = 7.4$  Hz, 1H), 7.87 (d,  $J = 7.5$  Hz, 1H), 7.75 (t,  $J = 7.5$  Hz, 1H), 7.46 (s, 1H), 7.37 (s, 1H), 7.17 (s, 1H), 6.00 (s, 2H), 5.55 (s, 2H), 3.94 (s, 3H), 3.90 (s, 3H), 2.79 (s, 3H).  $^{13}\text{C}$  NMR (75 MHz,  $\text{DMSO-}d_6$ )  $\delta$  197.8, 176.8, 156.5, 155.5, 149.7, 149.1, 146.1, 145.3, 135.9, 135.2, 135.1, 133.7, 130.8, 130.3, 129.9, 128.1, 126.5, 126.2, 121.2, 107.9, 107.6, 103.4, 67.6, 62.0, 56.8, 56.2, 30.7. HR-MS (ESI)  $m/z$ : calcd for  $\text{C}_{28}\text{H}_{26}\text{F}_3\text{NO}_6$  [ $\text{M} + \text{CH}_3\text{OH}$ ] $^+$  530.1785, found 530.1794.

(Z)-3-Acetyl-4-((6,7-dimethoxy-4-oxoisochroman-3-ylidene)methyl)-1-(4-(trifluoromethyl)benzyl)pyridin-1-ium Bromide (**10s**)

Brown solid, 90.9% yield.  $^1\text{H}$  NMR (300 MHz,  $\text{DMSO-}d_6$ )  $\delta$  9.67 (s, 1H), 9.09 (d,  $J = 7.0$  Hz, 1H), 8.72 (d,  $J = 6.7$  Hz, 1H), 7.86 (d,  $J = 8.3$  Hz, 2H), 7.80 (d,  $J = 8.3$  Hz, 2H), 7.43 (s, 1H), 7.34 (s, 1H), 7.13 (s, 1H), 5.98 (s, 2H), 5.52 (s, 2H), 3.91 (s, 3H), 3.86 (s, 3H), 2.75 (s, 3H).  $^{13}\text{C}$  NMR (75 MHz,  $\text{DMSO-}d_6$ )  $\delta$  197.7, 176.8, 156.5, 155.5, 149.7, 149.2, 146.1, 145.4, 139.2, 135.2, 135.1, 130.2, 130.2, 129.8, 128.1, 126.5, 126.5, 121.2, 118.8, 107.9, 107.6, 103.4, 67.6, 62.1, 56.8, 56.2, 30.6. HR-MS (ESI)  $m/z$ : calcd for  $\text{C}_{28}\text{H}_{26}\text{F}_3\text{NO}_6$  [ $\text{M} + \text{CH}_3\text{OH}$ ] $^+$  530.1785, found 530.1794.

### 3.1.13. Synthesis of Target Compounds **13a–13p**

To a solution of intermediate **12** in dry acetonitrile, benzyl bromide with different substituents (0.71 mmol, 3 eq) was added and stirred for 1–3 h at 85 °C. The solvent was removed under reduced pressure and recrystallized by ethyl acetate to give **13a–13p**.

(Z)-1-Benzyl-3-carbamoyl-4-((6,7-dimethoxy-4-oxoisochroman-3-ylidene)methyl)pyridin-1-ium Bromide (**13a**)

Red solid, 93.1% yield.  $^1\text{H}$  NMR (300 MHz,  $\text{DMSO-}d_6$ )  $\delta$  9.37 (s, 1H), 9.09 (d,  $J = 6.1$  Hz, 1H), 8.77 (d,  $J = 6.5$  Hz, 1H), 8.50 (s, 1H), 8.32 (s, 1H), 7.62 (s, 2H), 7.49 (s, 3H), 7.44 (s, 1H), 7.18 (s, 1H), 7.10 (s, 1H), 5.84 (s, 2H), 5.58 (s, 2H), 3.94 (s, 3H), 3.89 (s, 3H).  $^{13}\text{C}$  NMR (75 MHz,  $\text{DMSO-}d_6$ )  $\delta$  176.7, 165.3, 157.1, 155.5, 149.7, 147.8, 144.4, 143.2, 135.4, 135.1, 134.8, 129.8, 129.7, 129.7, 129.4, 129.4, 126.8, 121.1, 107.8, 107.6, 102.0, 67.7, 62.8, 56.8, 56.2. HR-MS (ESI)  $m/z$ : calcd for  $\text{C}_{25}\text{H}_{23}\text{N}_2\text{O}_5$  [ $\text{M}$ ] $^+$  431.1601, found 431.1606.

(Z)-3-Carbamoyl-4-((6,7-dimethoxy-4-oxoisochroman-3-ylidene)methyl)-1-(2-fluorobenzyl)pyridin-1-ium Bromide (**13b**)

Brown solid, 86.5% yield.  $^1\text{H}$  NMR (300 MHz,  $\text{DMSO-}d_6$ )  $\delta$  9.19 (s, 1H), 8.96 (d,  $J = 7.1$  Hz, 1H), 8.76 (d,  $J = 6.7$  Hz, 1H), 8.44 (s, 1H), 8.26 (s, 1H), 7.62 (t,  $J = 7.4$  Hz, 1H), 7.56–7.49 (m, 1H), 7.41 (s, 1H), 7.36 (d,  $J = 7.3$  Hz, 1H), 7.32 (d,  $J = 4.8$  Hz, 1H), 7.14 (s, 1H), 7.06 (s, 1H), 5.89 (s, 2H), 5.56 (s, 2H), 3.91 (s, 3H), 3.85 (s, 3H).  $^{13}\text{C}$  NMR (75 MHz,  $\text{DMSO-}d_6$ )  $\delta$  176.7, 165.3, 163.8, 162.6, 159.3, 157.3, 155.5, 149.7, 148.0, 144.7, 143.3, 135.4, 132.5, 131.9,

126.7, 125.8, 121.7, 121.1, 116.3, 107.6, 101.9, 67.7, 63.7, 56.8, 56.2. HR-MS (ESI)  $m/z$ : calcd for  $C_{25}H_{22}FN_2O_5 [M]^+$  449.1507, found 449.1511.

(Z)-3-Carbamoyl-4-((6,7-dimethoxy-4-oxoisochroman-3-ylidene)methyl)-1-(3-fluorobenzyl)pyridin-1-ium Bromide (**13c**)

Red solid, 90.2% yield.  $^1H$  NMR (300 MHz, DMSO- $d_6$ )  $\delta$  9.33 (s, 1H), 9.07 (d,  $J = 6.9$  Hz, 1H), 8.74 (d,  $J = 6.7$  Hz, 1H), 8.45 (s, 1H), 8.27 (s, 1H), 7.52 (dd,  $J = 7.8, 5.8$  Hz, 2H), 7.45 (d,  $J = 8.0$  Hz, 1H), 7.42 (s, 1H), 7.34–7.26 (m, 1H), 7.15 (s, 1H), 7.08 (s, 1H), 5.82 (s, 2H), 5.56 (s, 2H), 3.91 (s, 3H), 3.86 (s, 3H).  $^{13}C$  NMR (75 MHz, DMSO- $d_6$ )  $\delta$  176.7, 165.3, 164.3, 157.2, 155.5, 149.7, 148.0, 144.5, 143.3, 137.2, 135.3, 135.1, 131.7, 126.8, 125.6, 121.1, 116.6, 116.3, 107.8, 101.9, 92.5, 67.7, 62.0, 56.8, 56.2. HR-MS (ESI)  $m/z$ : calcd for  $C_{25}H_{22}FN_2O_5 [M]^+$  449.1507, found 449.1510.

(Z)-3-Carbamoyl-4-((6,7-dimethoxy-4-oxoisochroman-3-ylidene)methyl)-1-(4-fluorobenzyl)pyridin-1-ium Bromide (**13d**)

Red solid, 88.3% yield.  $^1H$  NMR (300 MHz, DMSO- $d_6$ )  $\delta$  9.27 (s, 1H), 9.02 (d,  $J = 6.5$  Hz, 1H), 8.72 (d,  $J = 6.8$  Hz, 1H), 8.45 (s, 1H), 8.27 (s, 1H), 7.68 (dd,  $J = 8.6, 5.4$  Hz, 2H), 7.41 (s, 1H), 7.31 (t,  $J = 8.8$  Hz, 2H), 7.12 (s, 1H), 7.06 (s, 1H), 5.77 (s, 2H), 5.54 (s, 2H), 3.91 (s, 3H), 3.85 (s, 3H).  $^{13}C$  NMR (75 MHz, DMSO- $d_6$ )  $\delta$  176.7, 165.3, 161.4, 157.1, 155.5, 149.7, 147.8, 144.3, 143.2, 135.3, 135.1, 132.1, 132.0, 131.0, 126.8, 121.1, 116.7, 116.4, 107.9, 107.6, 102.0, 67.7, 62.0, 56.8, 56.2. HR-MS (ESI)  $m/z$ : calcd for  $C_{25}H_{22}FN_2O_5 [M]^+$  449.1507, found 449.1510.

(Z)-3-Carbamoyl-1-(2-chlorobenzyl)-4-((6,7-dimethoxy-4-oxoisochroman-3-ylidene)methyl)pyridin-1-ium Bromide (**13e**)

Red solid, 89.3% yield.  $^1H$  NMR (300 MHz, DMSO- $d_6$ )  $\delta$  9.20 (s, 1H), 8.94 (d,  $J = 6.6$  Hz, 1H), 8.78 (d,  $J = 6.8$  Hz, 1H), 8.45 (s, 1H), 8.27 (s, 1H), 7.62 (d,  $J = 7.3$  Hz, 1H), 7.55–7.49 (m, 2H), 7.49–7.46 (m, 1H), 7.43 (s, 1H), 7.16 (s, 1H), 7.10 (s, 1H), 5.95 (s, 2H), 5.57 (s, 2H), 3.92 (s, 3H), 3.86 (s, 3H).  $^{13}C$  NMR (75 MHz, DMSO- $d_6$ )  $\delta$  176.7, 165.3, 157.3, 155.5, 149.7, 148.2, 144.8, 143.5, 140.5, 135.2, 135.1, 133.6, 132.0, 131.8, 130.5, 128.6, 126.7, 121.1, 107.9, 107.6, 101.9, 67.7, 60.8, 56.8, 56.2. HR-MS (ESI)  $m/z$ : calcd for  $C_{25}H_{22}ClN_2O_5 [M]^+$  465.1212, found 465.1214.

(Z)-3-Carbamoyl-1-(3-chlorobenzyl)-4-((6,7-dimethoxy-4-oxoisochroman-3-ylidene)methyl)pyridin-1-ium Bromide (**13f**)

Red solid, 90.8% yield.  $^1H$  NMR (300 MHz, DMSO- $d_6$ )  $\delta$  9.33 (s, 1H), 9.08 (d,  $J = 7.0$  Hz, 1H), 8.74 (d,  $J = 6.7$  Hz, 1H), 8.45 (s, 1H), 8.28 (s, 1H), 7.76 (s, 1H), 7.57 (s, 1H), 7.51 (d,  $J = 5.7$  Hz, 2H), 7.41 (d,  $J = 2.4$  Hz, 1H), 7.15 (s, 1H), 7.08 (s, 1H), 5.81 (s, 2H), 5.56 (s, 2H), 3.91 (s, 3H), 3.86 (s, 3H).  $^{13}C$  NMR (75 MHz, DMSO- $d_6$ )  $\delta$  176.7, 165.3, 157.2, 155.5, 149.7, 148.0, 144.5, 143.3, 136.9, 135.3, 135.1, 134.1, 131.5, 129.8, 129.4, 128.2, 126.9, 121.1, 107.8, 107.6, 101.9, 67.7, 61.9, 56.8, 56.2. HR-MS (ESI)  $m/z$ : calcd for  $C_{25}H_{22}ClN_2O_5 [M]^+$  465.1212, found 465.1217.

(Z)-3-Carbamoyl-1-(4-chlorobenzyl)-4-((6,7-dimethoxy-4-oxoisochroman-3-ylidene)methyl)pyridin-1-ium Bromide (**13g**)

Red solid, 90.5% yield.  $^1H$  NMR (300 MHz, DMSO- $d_6$ )  $\delta$  9.26 (s, 1H), 9.02 (d,  $J = 7.0$  Hz, 1H), 8.73 (d,  $J = 6.7$  Hz, 1H), 8.44 (s, 1H), 8.27 (s, 1H), 7.62 (d,  $J = 8.5$  Hz, 2H), 7.54 (d,  $J = 8.5$  Hz, 2H), 7.41 (s, 1H), 7.12 (s, 1H), 7.06 (s, 1H), 5.78 (s, 2H), 5.55 (s, 2H), 3.90 (s, 3H), 3.85 (s, 3H).  $^{13}C$  NMR (75 MHz, DMSO- $d_6$ )  $\delta$  176.7, 165.3, 157.1, 155.5, 149.7, 147.9, 144.4, 143.2, 135.3, 135.1, 134.6, 133.6, 131.5, 131.5, 129.6, 129.6, 126.8, 121.1, 107.8, 107.5, 101.9, 67.7, 61.9, 56.8, 56.2. HR-MS (ESI)  $m/z$ : calcd for  $C_{25}H_{22}ClN_2O_5 [M]^+$  465.1212, found 465.1215.

(Z)-1-(2-Bromobenzyl)-3-carbamoyl-4-((6,7-dimethoxy-4-oxoisochroman-3-ylidene)methyl)pyridin-1-ium Bromide (**13h**)

Brown solid, 91.2% yield.  $^1H$  NMR (300 MHz, DMSO- $d_6$ )  $\delta$  9.23 (s, 1H), 8.94 (d,  $J = 7.1$  Hz, 1H), 8.81 (d,  $J = 6.8$  Hz, 1H), 8.49 (s, 1H), 8.31 (s, 1H), 7.82 (d,  $J = 7.8$  Hz, 1H), 7.54 (t,  $J = 7.0$  Hz, 1H), 7.49–7.43 (m, 2H), 7.40 (d,  $J = 7.4$  Hz, 1H), 7.19 (s, 1H), 7.13 (s, 1H), 5.94 (s, 2H), 5.60 (s, 2H), 3.94 (s, 3H), 3.89 (s, 3H).  $^{13}C$  NMR (75 MHz, DMSO- $d_6$ )  $\delta$  176.7, 165.3, 157.4, 155.5, 149.7, 148.2, 144.9, 143.6, 135.2, 135.1, 133.8, 133.6, 131.8, 131.6, 129.1, 126.7, 123.8, 121.1, 107.8, 107.6, 101.9, 67.7, 62.8, 56.8, 56.2. HR-MS (ESI)  $m/z$ : calcd for  $C_{25}H_{22}BrN_2O_5 [M]^+$  509.0707, found 509.0705.

(Z)-1-(3-Bromobenzyl)-3-carbamoyl-4-((6,7-dimethoxy-4-oxoisochroman-3-ylidene)methyl)pyridin-1-ium Bromide (**13i**)

Yellow solid, 89.6% yield.  $^1\text{H}$  NMR (300 MHz, DMSO- $d_6$ )  $\delta$  9.35 (s, 1H), 9.10 (d,  $J = 6.8$  Hz, 1H), 8.77 (d,  $J = 6.8$  Hz, 1H), 8.48 (s, 1H), 8.32 (s, 1H), 7.92 (s, 1H), 7.72–7.61 (m, 2H), 7.52–7.42 (m, 2H), 7.18 (s, 1H), 7.10 (s, 1H), 5.82 (s, 2H), 5.59 (s, 2H), 3.94 (s, 3H), 3.88 (s, 3H).  $^{13}\text{C}$  NMR (75 MHz, DMSO- $d_6$ )  $\delta$  176.7, 165.3, 157.2, 155.5, 149.7, 148.0, 144.5, 143.3, 137.1, 135.3, 135.1, 132.7, 132.3, 131.8, 128.6, 126.9, 122.7, 121.1, 107.9, 107.6, 101.9, 67.7, 61.9, 56.8, 56.2. HR-MS (ESI)  $m/z$ : calcd for  $\text{C}_{25}\text{H}_{22}\text{BrN}_2\text{O}_5$   $[\text{M}]^+$  509.0707, found 509.0705.

(Z)-1-(4-Bromobenzyl)-3-carbamoyl-4-((6,7-dimethoxy-4-oxoisochroman-3-ylidene)methyl)pyridin-1-ium Bromide (**13j**)

Yellow solid, 88.2% yield.  $^1\text{H}$  NMR (300 MHz, DMSO- $d_6$ )  $\delta$  9.33 (s, 1H), 9.07 (d,  $J = 6.9$  Hz, 1H), 8.75 (d,  $J = 6.8$  Hz, 1H), 8.47 (s, 1H), 8.30 (s, 1H), 7.71 (d,  $J = 8.4$  Hz, 2H), 7.59 (d,  $J = 8.4$  Hz, 2H), 7.43 (s, 1H), 7.17 (s, 1H), 7.09 (s, 1H), 5.81 (s, 2H), 5.58 (s, 2H), 3.93 (s, 3H), 3.88 (s, 3H).  $^{13}\text{C}$  NMR (75 MHz, DMSO- $d_6$ )  $\delta$  176.7, 165.3, 157.1, 155.5, 149.7, 147.9, 144.5, 143.3, 135.3, 135.1, 134.0, 132.5, 132.5, 131.7, 131.7, 126.8, 123.3, 121.1, 107.8, 107.6, 101.9, 67.7, 62.0, 56.8, 56.2. HR-MS (ESI)  $m/z$ : calcd for  $\text{C}_{25}\text{H}_{22}\text{BrN}_2\text{O}_5$   $[\text{M}]^+$  509.0707, found 509.0705.

(Z)-3-Carbamoyl-4-((6,7-dimethoxy-4-oxoisochroman-3-ylidene)methyl)-1-(2-methylbenzyl)pyridin-1-ium Bromide (**13k**)

Yellow solid, 89.8% yield.  $^1\text{H}$  NMR (300 MHz, DMSO- $d_6$ )  $\delta$  9.20 (s, 1H), 8.87 (d,  $J = 7.1$  Hz, 1H), 8.79 (d,  $J = 6.8$  Hz, 1H), 8.50 (s, 1H), 8.31 (s, 1H), 7.45 (s, 1H), 7.37 (t,  $J = 7.1$  Hz, 2H), 7.31 (d,  $J = 6.5$  Hz, 1H), 7.24–7.16 (m, 2H), 7.12 (s, 1H), 5.88 (s, 2H), 5.59 (s, 2H), 3.94 (s, 3H), 3.89 (s, 3H), 2.35 (s, 3H).  $^{13}\text{C}$  NMR (75 MHz, DMSO- $d_6$ )  $\delta$  176.7, 165.3, 157.2, 155.5, 149.7, 147.9, 144.6, 143.3, 137.4, 135.2, 135.1, 132.7, 131.3, 129.8, 129.5, 127.1, 126.8, 121.1, 107.8, 107.6, 101.9, 67.7, 61.1, 56.8, 56.2, 19.4. HR-MS (ESI)  $m/z$ : calcd for  $\text{C}_{26}\text{H}_{25}\text{N}_2\text{O}_5$   $[\text{M}]^+$  445.1758, found 445.1765.

(Z)-3-Carbamoyl-4-((6,7-dimethoxy-4-oxoisochroman-3-ylidene)methyl)-1-(3-methylbenzyl)pyridin-1-ium Bromide (**13l**)

Yellow solid, 87.6% yield.  $^1\text{H}$  NMR (300 MHz, DMSO- $d_6$ )  $\delta$  9.34 (s, 1H), 9.08 (d,  $J = 6.8$  Hz, 1H), 8.76 (d,  $J = 6.7$  Hz, 1H), 8.50 (s, 1H), 8.32 (s, 1H), 7.44 (s, 2H), 7.42–7.35 (m, 2H), 7.28 (d,  $J = 6.6$  Hz, 1H), 7.18 (s, 1H), 7.10 (s, 1H), 5.78 (s, 2H), 5.58 (s, 2H), 3.94 (s, 3H), 3.88 (s, 3H), 2.36 (s, 3H).  $^{13}\text{C}$  NMR (75 MHz, DMSO- $d_6$ )  $\delta$  176.8, 165.4, 157.2, 155.6, 149.8, 147.9, 144.5, 143.2, 139.1, 135.4, 135.2, 134.7, 130.5, 130.0, 129.7, 126.9, 126.6, 121.2, 107.9, 107.7, 102.1, 67.8, 62.9, 56.9, 56.3, 21.5. HR-MS (ESI)  $m/z$ : calcd for  $\text{C}_{26}\text{H}_{25}\text{N}_2\text{O}_5$   $[\text{M}]^+$  445.1758, found 445.1758.

(Z)-3-Carbamoyl-4-((6,7-dimethoxy-4-oxoisochroman-3-ylidene)methyl)-1-(4-methylbenzyl)pyridin-1-ium Bromide (**13m**)

Yellow solid, 88.1% yield.  $^1\text{H}$  NMR (300 MHz, DMSO- $d_6$ )  $\delta$  9.32 (s, 1H), 9.06 (d,  $J = 7.1$  Hz, 1H), 8.75 (d,  $J = 6.8$  Hz, 1H), 8.48 (s, 1H), 8.31 (s, 1H), 7.52 (d,  $J = 8.0$  Hz, 2H), 7.44 (s, 1H), 7.30 (d,  $J = 7.9$  Hz, 2H), 7.17 (s, 1H), 7.09 (s, 1H), 5.77 (s, 2H), 5.55 (d,  $J = 14.5$  Hz, 2H), 3.94 (s, 3H), 3.88 (s, 3H), 2.34 (s, 3H).  $^{13}\text{C}$  NMR (75 MHz, DMSO- $d_6$ )  $\delta$  176.7, 165.3, 157.0, 155.5, 149.7, 147.7, 144.3, 143.0, 139.4, 135.4, 135.1, 131.8, 130.2, 130.2, 129.5, 129.5, 126.8, 121.1, 107.8, 107.6, 102.0, 67.7, 62.7, 56.8, 56.2, 21.2. HR-MS (ESI)  $m/z$ : calcd for  $\text{C}_{26}\text{H}_{25}\text{N}_2\text{O}_5$   $[\text{M}]^+$  445.1758, found 445.1762.

(Z)-3-Carbamoyl-4-((6,7-dimethoxy-4-oxoisochroman-3-ylidene)methyl)-1-(2-(trifluoromethyl)benzyl)pyridin-1-ium Bromide (**13n**)

Yellow solid, 89.5% yield.  $^1\text{H}$  NMR (300 MHz, DMSO- $d_6$ )  $\delta$  9.24 (s, 1H), 8.91 (d,  $J = 6.8$  Hz, 1H), 8.82 (d,  $J = 6.7$  Hz, 1H), 8.50 (s, 1H), 8.30 (s, 1H), 7.96 (d,  $J = 7.6$  Hz, 1H), 7.81 (t,  $J = 7.4$  Hz, 1H), 7.73 (t,  $J = 7.3$  Hz, 1H), 7.46 (s, 1H), 7.32 (d,  $J = 7.5$  Hz, 1H), 7.18 (d,  $J = 7.8$  Hz, 2H), 6.09 (s, 2H), 5.61 (s, 2H), 3.95 (s, 3H), 3.89 (s, 3H).  $^{13}\text{C}$  NMR (75 MHz, DMSO- $d_6$ )  $\delta$  176.6, 165.2, 157.4, 155.5, 149.7, 148.4, 145.1, 143.9, 135.2, 135.1, 134.1, 132.0, 130.7, 130.2, 127.3, 126.7, 126.3, 122.6, 121.1, 107.8, 107.6, 101.8, 67.7, 59.5, 56.8, 56.2. HR-MS (ESI)  $m/z$ : calcd for  $\text{C}_{26}\text{H}_{22}\text{F}_3\text{N}_2\text{O}_5$   $[\text{M}]^+$  499.1475, found 499.1479.

(Z)-3-Carbamoyl-4-((6,7-dimethoxy-4-oxoisochroman-3-ylidene)methyl)-1-(3-(trifluoromethyl)benzyl)pyridin-1-ium Bromide (**13o**)



Yellow solid, 87.4% yield.  $^1\text{H}$  NMR (300 MHz,  $\text{DMSO-}d_6$ )  $\delta$  9.38 (s, 1H), 9.13 (d,  $J = 6.8$  Hz, 1H), 8.78 (d,  $J = 6.7$  Hz, 1H), 8.46 (s, 1H), 8.30 (s, 1H), 8.12 (s, 1H), 7.94 (d,  $J = 7.7$  Hz, 1H), 7.85 (d,  $J = 7.8$  Hz, 1H), 7.74 (t,  $J = 7.8$  Hz, 1H), 7.44 (s, 1H), 7.17 (s, 1H), 7.11 (s, 1H), 5.92 (s, 2H), 5.58 (s, 2H), 3.94 (s, 3H), 3.88 (s, 3H).  $^{13}\text{C}$  NMR (75 MHz,  $\text{DMSO-}d_6$ )  $\delta$  176.7, 165.3, 157.2, 155.5, 149.7, 148.0, 144.5, 143.4, 135.9, 135.3, 135.1, 133.8, 130.8, 130.3, 129.9, 126.9, 126.6, 122.6, 121.1, 107.8, 107.6, 101.9, 67.7, 62.0, 56.8, 56.2. HR-MS (ESI)  $m/z$ : calcd for  $\text{C}_{26}\text{H}_{22}\text{F}_3\text{N}_2\text{O}_5$   $[\text{M}]^+$  499.1475, found 499.1479.

(Z)-3-Carbamoyl-4-((6,7-dimethoxy-4-oxoisochroman-3-ylidene)methyl)-1-(4-(trifluoromethyl)benzyl)pyridin-1-ium Bromide (**13p**)

Brown solid, 87.9% yield.  $^1\text{H}$  NMR (300 MHz,  $\text{DMSO-}d_6$ )  $\delta$  9.38 (s, 1H), 9.12 (d,  $J = 6.8$  Hz, 1H), 8.79 (d,  $J = 6.7$  Hz, 1H), 8.49 (s, 1H), 8.31 (s, 1H), 7.89 (d,  $J = 8.3$  Hz, 2H), 7.84 (d,  $J = 8.3$  Hz, 2H), 7.45 (s, 1H), 7.18 (s, 1H), 7.13 (s, 1H), 5.97 (s, 2H), 5.60 (s, 2H), 3.95 (s, 3H), 3.89 (s, 3H).  $^{13}\text{C}$  NMR (75 MHz,  $\text{DMSO-}d_6$ )  $\delta$  176.7, 165.3, 157.2, 155.5, 149.7, 148.1, 144.7, 143.5, 139.2, 135.3, 135.1, 130.2, 130.2, 129.8, 126.9, 126.5, 126.4, 126.2, 121.1, 107.8, 107.6, 101.9, 67.7, 62.0, 56.8, 56.2. HR-MS (ESI)  $m/z$ : calcd for  $\text{C}_{26}\text{H}_{22}\text{F}_3\text{N}_2\text{O}_5$   $[\text{M}]^+$  499.1475, found 499.1484.

### 3.2. Biological Evaluation

#### 3.2.1. Inhibition of eeAChE

AChE activity was measured by the ELISA method using AChE enzyme from *Electrophorus electricus* (eeAChE) (C3389, Merck, Kenilworth, NJ, USA) [36]. AChE solution (2 U/mL) was prepared with 0.1 M phosphate buffer (pH 8.0) firstly. Varied concentrations of test compounds (20  $\mu\text{L}$ ), 1 mM 5'-dithiobis (2-nitrobenzoic acid) (DTNB) solution (100  $\mu\text{L}$ ), and AChE solution (40  $\mu\text{L}$ ) were added in order to each well of a 96-well plate. After incubation for 15 min at 37  $^\circ\text{C}$ , the reaction was initiated by adding 20  $\mu\text{L}$  of acetylthiocholine iodide (1 mM) to the mixed solution. The absorbance of each plate was instantly measured at 405 nm using a microplate reader. The inhibition of each compound was estimated using the formula  $(1 - \text{Ai}/\text{Ac}) \times 100$ , where Ai and Ac represent the absorbance of AChE in the presence and absence of inhibitors, respectively. Each experiment was replicated three times. Plotting curves of log concentration via percentage of inhibition, the  $\text{IC}_{50}$  values of all tested compounds were graphically analyzed (Graph Pad Prism 8.0).

#### 3.2.2. Kinetic Study of AChE Inhibition

Kinetic study of AChE inhibition was carried out using Ellman's method [30], which is the same as the AChE assay, to determine the kinetic mechanism of chemical inhibition. The kinetic inhibition of compound **10a** was analyzed at concentrations of 0.8 and 1.6 nM. Lineweaver–Burk reciprocal plots were created by graphing  $1/\text{velocity}$  vs.  $1/[\text{substrate}]$  at various concentrations of substrate acetylthiocholine. The software GraphPad Prism 8.0 was used to analyze the data.

#### 3.2.3. In Vitro Antioxidant Activity Assay

Compound **10a** was tested for free radical-scavenging activity using 1,1-diphenyl-2-picryl-hydrazyl (DPPH) (D9132, Merck, Kenilworth, NJ, USA) [37]. To make a 0.1 mM concentration of DPPH stock solution, DPPH was dissolved in methanol. In a 96-well plate, 10  $\mu\text{L}$  of the test sample at 100  $\mu\text{M}$  and 90  $\mu\text{L}$  of DPPH solution were added into each well. Trolox was used as a reference. The absorbance was measured at 545 nm after 30 min of reaction at 25  $^\circ\text{C}$ .

#### 3.2.4. Self-Induced $\text{A}\beta$ Aggregation Inhibition by Thioflavin T Assay

A total of 1 mg  $\text{A}\beta$  (P9001, Beyotime, Shanghai, China) was dissolved in 1 mL of hexafluoroisopropanol and aliquoted into 50  $\mu\text{L}$  per tube. Then, 20  $\mu\text{L}$  of DMSO was added into one tube of  $\text{A}\beta$  solution. The test compound was prepared as a 10 mM of stock solution with DMSO and diluted to 50  $\mu\text{M}$  with PBS (including the control). Then, 20  $\mu\text{L}$  of the test compound and 20  $\mu\text{L}$  of the  $\text{A}\beta$  solution were added to a 96-well black plate, which was

gently tapped to mix the solution, covered tightly and sealed with black tape to prevent evaporation of the solvent, and left in the dark at room temperature for 24 h. Then, 160  $\mu\text{L}$  of THT solution at a concentration of 5  $\mu\text{M}$  was added and the fluorescence absorption was measured at an excitation wavelength of 445 nm and an emission wavelength of 490 nm. The software GraphPad Prism 8.0 was used to analyze the data.

### 3.2.5. Cytotoxicity Assay on SH-SY5Y Cells

SH-SY5Y cells were grown in a 25  $\text{cm}^2$  culture flask in fresh MEM/F12 medium, supplemented with 10% fetal bovine serum, 100 U/mL penicillin, and 100 g/mL streptomycin, and incubated at 37  $^\circ\text{C}$  with 5%  $\text{CO}_2$ . Cells were seeded at a density of  $1 \times 10^4$  cells per well in a 96-well plate. After incubation for 24 h, medium was removed. Compounds **10a** or **13b** (10, 20, 50  $\mu\text{M}$ ) were prepared with serum-free media and added into each well of the plate for 24 h. After 24 h treatment, 10  $\mu\text{L}$  of 3-(4,5-dimethyl-2-thiazolyl)-2,5-diphenyl-2-H-tetrazolium bromide was added into each well. After 4 h of incubation at 37  $^\circ\text{C}$ , 100  $\mu\text{L}$  of DMSO was added to dissolve the formazan crystals, and the mixture's absorbance was measured at 490 nm under a microplate reader (FC/K3, Thermo, Waltham, MA, USA). The survival rate was estimated using the formula  $A_e/A_b \times 100\%$ , where  $A_e$  and  $A_b$  represent the absorbance of SH-SY5Y cells in the presence and absence of the tested drugs, respectively. Each experiment was replicated three times.

### 3.2.6. Molecular Docking Study

The protein structure of AChE (PDB ID: 4EY7) was downloaded from Protein Data Bank (<https://www.rcsb.org>) (accessed on 15 January 2022). AChE was refined and an active pocket for AChE was defined using the protein preparation and receptor grid generating components of Schrodinger software. To improve tiny molecule structures, the ligand preparation module was employed. Finally, AChE was docked using the ligand docking module.

## 4. Conclusions

In conclusion, by fusing the pharmacophores of ( $\pm$ )-XJP-B and donepezil, a series of novel *isochroman-4-one* derivatives were designed, synthesized and evaluated as AChE inhibitors. The AChE inhibitory activity of these new compounds was overall strong, with  $\text{IC}_{50}$  values in the nanomolar range, and representative compound **10a** [(Z)-3-acetyl-1-benzyl-4-((6,7-dimethoxy-4-oxoisochroman-3-ylidene)methyl)pyridin-1-ium bromide] was the most potent molecule ( $\text{IC}_{50} = 1.61$  nM). Diverse substituents, including electron-donating groups and electron-drawing groups, were introduced into different positions on the benzene ring of the target compounds to investigate the substituent effects (the electronic effect, steric effect and position of substituted groups) and systematically analyze the structure activity relationships. Further molecular docking studies revealed that compound **10a** occupies the active pocket of AChE well, forming secondary bonds with the pocket's amino acid residues. With the results of low cytotoxicity, anti-oxidation and inhibition of self-induced  $A\beta$  aggregation, it is strongly suggested that compound **10a** is a promising lead compound to be further studied for discovery and development of novel and effective anti-AD drugs.

**Supplementary Materials:** The following supporting information can be downloaded at: <https://www.mdpi.com/article/10.3390/molecules27103090/s1>, The spectra of  $^1\text{H-NMR}$  and  $^{13}\text{C-NMR}$  for the target compounds.

**Author Contributions:** X.L., P.Z. and J.X. conceived and designed the experiments; X.L., P.Z., Y.J. and J.L. (Junda Li) performed the synthesis; T.L., L.L. and Z.Z. performed the activity tests, and X.L. and Y.J. performed molecular docking studies and performed analysis studies; X.L., J.X., H.Y., J.L. (Jie Liu) and Z.Z. wrote the paper. All authors have read and agreed to the published version of the manuscript.

**Funding:** The authors thank the National Natural Science Foundation of China (No. 81874289) for financial support. This study was financed in part by the “Double First-Class” University project CPU2018GY04, China Pharmaceutical University.

**Institutional Review Board Statement:** Not applicable.

**Informed Consent Statement:** Not applicable.

**Data Availability Statement:** The data presented in this study are available within the article and Supplementary Materials.

**Conflicts of Interest:** The authors declare no conflict of interest.

**Sample Availability:** Sample of the compounds are not available from authors.

## References

1. Zhang, P.; Xu, S.; Zhu, Z.; Xu, J. Multi-target design strategies for the improved treatment of Alzheimer’s disease. *Eur. J. Med. Chem.* **2019**, *176*, 228–247. [[CrossRef](#)] [[PubMed](#)]
2. Kaur, S.; Bansal, Y. Design, molecular Docking, synthesis and evaluation of xanthoxylin hybrids as dual inhibitors of IL-6 and acetylcholinesterase for Alzheimer’s disease. *Bioorg. Chem.* **2022**, *121*, 105670. [[CrossRef](#)] [[PubMed](#)]
3. Verma, A.; Kumar Waiker, D.; Bhardwaj, B.; Saraf, P.; Shrivastava, S.K. The molecular mechanism, targets, and novel molecules in the treatment of Alzheimer’s disease. *Bioorg. Chem.* **2022**, *119*, 105562. [[CrossRef](#)] [[PubMed](#)]
4. Behl, C. The search for novel avenues for the therapy and prevention of Alzheimer’s disease. *Drug News Perspec.* **2006**, *19*, 5–12. [[CrossRef](#)]
5. Friedlander, A.H.; Norman, D.C.; Mahler, M.E.; Norman, K.M.; Yagiela, J.A. Alzheimer’s disease: Psychopathology, medical management and dental implications. *J. Am. Dent. Assoc.* **2006**, *137*, 1240–1251. [[CrossRef](#)] [[PubMed](#)]
6. Kumar, A.; Seghal, N.; Padi, S.V.; Naidu, P.S. Differential effects of cyclooxygenase inhibitors on intracerebroventricular colchicine-induced dysfunction and oxidative stress in rats. *Eur. J. Pharmacol.* **2006**, *551*, 58–66. [[CrossRef](#)]
7. Tiwari, V.; Kuhad, A.; Bishnoi, M.; Chopra, K. Chronic treatment with tocotrienol, an isoform of vitamin E, prevents intracerebroventricular streptozotocin-induced cognitive impairment and oxidative-nitrosative stress in rats. *Pharmacol. Biochem. Behav.* **2009**, *93*, 183–189. [[CrossRef](#)]
8. Ozkay, U.D.; Can, O.D.; Ozkay, Y.; Oztürk, Y. Effect of benzothiazole/piperazine derivatives on intracerebroventricular streptozotocin-induced cognitive deficits. *Pharmacol. Rep.* **2012**, *64*, 834–847. [[CrossRef](#)]
9. Brookmeyer, R.; Gray, S.; Kawas, C. Projections of Alzheimer’s disease in the United States and the public health impact of delaying disease onset. *Am. J. Public Health* **1998**, *88*, 1337–1342. [[CrossRef](#)]
10. Fan, L.; Mao, C.; Hu, X.; Zhang, S.; Yang, Z.; Hu, Z.; Sun, H.; Fan, Y.; Dong, Y.; Yang, J.; et al. New Insights Into the Pathogenesis of Alzheimer’s Disease. *Front. Neurol.* **2019**, *10*, 1312. [[CrossRef](#)]
11. Kandimalla, R.; Reddy, P.H. Therapeutics of Neurotransmitters in Alzheimer’s Disease. *J. Alzheimers Dis.* **2017**, *57*, 1049–1069. [[CrossRef](#)] [[PubMed](#)]
12. Yao, H.; Uras, G.; Zhang, P.; Xu, S.; Yin, Y.; Liu, J.; Qin, S.; Li, X.; Allen, S.; Bai, R.; et al. Discovery of Novel Tacrine-Pyrimidone Hybrids as Potent Dual AChE/GSK-3 Inhibitors for the Treatment of Alzheimer’s Disease. *J. Med. Chem.* **2021**, *64*, 7483–7506. [[CrossRef](#)] [[PubMed](#)]
13. Selkoe, D.J. The molecular pathology of Alzheimer’s disease. *Neuron* **1991**, *6*, 487–498. [[CrossRef](#)]
14. Frost, B.; Jacks, R.L.; Diamond, M.I. Propagation of tau misfolding from the outside to the inside of a cell. *J. Biol. Chem.* **2009**, *284*, 12845–12852. [[CrossRef](#)]
15. Adlard, P.A.; Bush, A.I. Metals and Alzheimer’s disease. *J. Alzheimers Dis.* **2006**, *10*, 145–163. [[CrossRef](#)]
16. Popugaeva, E.; Pchitskaya, E.; Bezprozvanny, I. Dysregulation of neuronal calcium homeostasis in Alzheimer’s disease—A therapeutic opportunity? *Biochem. Biophys. Res. Commun.* **2017**, *483*, 998–1004. [[CrossRef](#)]
17. Perry, V.H.; Holmes, C. Microglial priming in neurodegenerative disease. *Nat. Rev. Neurol.* **2014**, *10*, 217–224. [[CrossRef](#)]
18. Butterfield, D.A.; Halliwell, B. Oxidative stress, dysfunctional glucose metabolism and Alzheimer disease. *Nat. Rev. Neurosci.* **2019**, *20*, 148–160. [[CrossRef](#)]
19. Maspero, M.; Volpato, D.; Cirillo, D.; Yuan Chen, N.; Messerer, R.; Sottriffer, C.; De Amici, M.; Holzgrabe, U.; Dallanoce, C. Tacrine-xanomeline and tacrine-iperoxo hybrid ligands: Synthesis and biological evaluation at acetylcholinesterase and M1 muscarinic acetylcholine receptors. *Bioorg. Chem.* **2020**, *96*, 103633. [[CrossRef](#)]
20. Verma, S.; Kumar, A.; Tripathi, T.; Kumar, A. Muscarinic and nicotinic acetylcholine receptor agonists: Current scenario in Alzheimer’s disease therapy. *J. Pharm. Pharmacol.* **2018**, *70*, 985–993. [[CrossRef](#)]
21. Scheltens, P.; Feldman, H.J.T.L.N. Treatment of Alzheimer’s disease; current status and new perspectives. *Lancet Neurol.* **2003**, *2*, 539–547.
22. Messerer, R.; Dallanoce, C.; Matera, C.; Wehle, S.; Flammini, L.; Chirinda, B.; Bock, A.; Irmen, M.; Tränkle, C.; Barocelli, E.J.M. Novel bipharmacophoric inhibitors of the cholinesterases with affinity to the muscarinic receptors M1 and M2. *Med. Chem. Commun.* **2017**, *8*, 1346–1359. [[CrossRef](#)] [[PubMed](#)]

23. Arce, M.P.; Rodríguez-Franco, M.I.; González-Muñoz, G.C.; Pérez, C.; López, B.; Villarroya, M.; López, M.G.; García, A.G.; Conde, S. Neuroprotective and cholinergic properties of multifunctional glutamic acid derivatives for the treatment of Alzheimer's disease. *J. Med. Chem.* **2009**, *52*, 7249–7257. [[CrossRef](#)] [[PubMed](#)]
24. Basiri, A.; Xiao, M.; McCarthy, A.; Dutta, D.; Byrareddy, S.N.; Conda-Sheridan, M. Design and synthesis of new piperidone grafted acetylcholinesterase inhibitors. *Bioorg. Med. Chem. Lett.* **2017**, *27*, 228–231. [[CrossRef](#)]
25. He, Q.; Liu, J.; Lan, J.; Ding, J.; Sun, Y.; Fang, Y.; Jiang, N.; Yang, Z.; Sun, L.; Jin, Y.; et al. Coumarin-dithiocarbamate hybrids as novel multitarget AChE and MAO-B inhibitors against Alzheimer's disease: Design, synthesis and biological evaluation. *Bioorg. Chem.* **2018**, *81*, 512–528. [[CrossRef](#)]
26. Sang, Z.; Wang, K.; Wang, H.; Yu, L.; Wang, H.; Ma, Q.; Ye, M.; Han, X.; Liu, W. Design, synthesis and biological evaluation of phthalimide-alkylamine derivatives as balanced multifunctional cholinesterase and monoamine oxidase-B inhibitors for the treatment of Alzheimer's disease. *Bioorg. Med. Chem. Lett.* **2017**, *27*, 5053–5059. [[CrossRef](#)]
27. Zhu, J.; Wang, L.N.; Cai, R.; Geng, S.Q.; Dong, Y.F.; Liu, Y.M. Design, synthesis, evaluation and molecular modeling study of 4-N-phenylaminoquinolines for Alzheimer disease treatment. *Bioorg. Med. Chem. Lett.* **2019**, *29*, 1325–1329. [[CrossRef](#)]
28. Qian, H.; Huang, W. A new isochroman-4-one derivative from the peel of *Musa sapientum* L. and its total synthesis. *Chin. Chem. Lett.* **2007**, *18*, 1227–1230. [[CrossRef](#)]
29. Bai, R.; Yang, X.; Zhu, Y.; Zhou, Z.; Xie, W.; Yao, H.; Jiang, J.; Liu, J.; Shen, M.; Wu, X.; et al. Novel nitric oxide-releasing isochroman-4-one derivatives: Synthesis and evaluation of antihypertensive activity. *Bioorg. Med. Chem.* **2012**, *20*, 6848–6855. [[CrossRef](#)]
30. Shuai, W.; Li, W.; Yin, Y.; Yang, L.; Xu, F.; Xu, S.; Yao, H.; Zhu, Z.; Xu, J. Design, synthesis and molecular modeling of isothiochromanone derivatives as acetylcholinesterase inhibitors. *Future Med. Chem.* **2019**, *11*, 2687–2699. [[CrossRef](#)]
31. Wang, C.; Wu, Z.; Cai, H.; Xu, S.; Liu, J.; Jiang, J.; Yao, H.; Wu, X.; Xu, J. Design, synthesis, biological evaluation and docking study of 4-isochromanone hybrids bearing N-benzyl pyridinium moiety as dual binding site acetylcholinesterase inhibitors. *Bioorg. Med. Chem. Lett.* **2015**, *25*, 5212–5216. [[CrossRef](#)] [[PubMed](#)]
32. Wang, J.; Wang, C.; Wu, Z.; Li, X.; Xu, S.; Liu, J.; Lan, Q.; Zhu, Z.; Xu, J. Design, synthesis, biological evaluation, and docking study of 4-isochromanone hybrids bearing N-benzyl pyridinium moiety as dual binding site acetylcholinesterase inhibitors (part II). *Chem. Biol. Drug Des.* **2018**, *91*, 756–762. [[CrossRef](#)] [[PubMed](#)]
33. Wang, Y.; Yang, Y.; Hong, K.H.; Ning, Y.; Yu, P.; Ren, J.; Ji, M.; Cai, J. Design, synthesis and evaluation of a novel metal chelator as multifunctional agents for the treatment of Alzheimer's disease. *Bioorg. Chem.* **2019**, *87*, 720–727. [[CrossRef](#)] [[PubMed](#)]
34. Son, S.H.; Do, J.M.; Yoo, J.N.; Lee, H.W.; Kim, N.K.; Yoo, H.S.; Gee, M.S.; Kim, J.H.; Seong, J.H.; Inn, K.S.; et al. Identification of ortho catechol-containing isoflavone as a privileged scaffold that directly prevents the aggregation of both amyloid  $\beta$  plaques and tau-mediated neurofibrillary tangles and its in vivo evaluation. *Bioorg. Chem.* **2021**, *113*, 105022. [[CrossRef](#)] [[PubMed](#)]
35. Cheng, F.; Li, W.; Zhou, Y.; Shen, J.; Wu, Z.; Liu, G.; Lee, P.W.; Tang, Y. admetSAR: A comprehensive source and free tool for assessment of chemical ADMET properties. *J. Chem. Inf. Model.* **2012**, *52*, 3099–3105. [[CrossRef](#)]
36. Ellman, G.L.; Courtney, K.D.; Andres, V., Jr.; Feather-Stone, R.M. A new and rapid colorimetric determination of acetylcholinesterase activity. *Biochem. Pharmacol.* **1961**, *7*, 88–95. [[CrossRef](#)]
37. Haghijoo, Z.; Firuzi, O.; Hemmateenejad, B.; Emami, S.; Edraki, N.; Miri, R. Synthesis and biological evaluation of quinazolinone-based hydrazones with potential use in Alzheimer's disease. *Bioorg. Chem.* **2017**, *74*, 126–133. [[CrossRef](#)]